BỘ GIÁO DỤC VÀ ĐÀO TẠO
TRƯỜNG ĐẠI HỌC SƯ PHẠM KỸ THUẬT
THÀNH PHỐ HỒ CHÍ MINH

TRƯƠNG QUANG PHÚC

NGHIÊN CỨU MẠNG THÔNG TIN VÔ TUYẾN QUA KÊNH TRUYỀN VỚI CÁC BỀ MẶT PHẢN XẠ THÔNG MINH

CÔNG TRÌNH NGHIÊN CỨU
NGÀNH: KỸ THUẬT ĐIỆN TỬ

Tp. Hồ Chí Minh, tháng 08/2025

DANH MỤC CÁC CÔNG TRÌNH ĐÃ CÔNG BỐ

*(C1) Bài báo được trình bày tại hội nghị **INISCOM 2022** và được đăng trong **Book series LNICST** của Springer **(Q4)***

***P.Q. Truong,** V.-C. Phan. (2022). Reconfigurable Intelligent Surfaces for Downlink Cellular Networks. In Industrial Networks and Intelligent Systems. INISCOM 2022. Lecture Notes of the Institute for Computer Sciences, Social Informatics and Telecommunications Engineering, vol 444. Springer, Cham. https://doi.org/10.1007/978-3-031-08878-0_2*

*(J1) Bài báo được xuất bản trên tạp chí **EAI Endorsed Transactions on Industrial Networks and Intelligent Systems** xếp hạng **Q3** theo **Scopus***

***P. Q. Truong**, T. Do-Duy, V.-C. Phan and A. Masaracchia, "Jointly power allocation and phase shift optimization for RIS empowered downlink cellular networks," EAI Endorsed Transactions on Industrial Networks and Intelligent Systems, vol. 10, no. 4, 2023, http://dx.doi.org/10.4108/eetinis.v10i4.4359*

*(J2) Bài báo được xuất bản trên tạp chí **IEEE Access** xếp hạng **Q1 (SCIE)***

***P. Q. Truong**, T. Do-Duy, A. Masaracchia, N.-S. Vo, V.-C. Phan, D.-B. Ha và T. Q. Duong, "Computation Offloading and Resource Allocation Optimization for Mobile Edge Computing-Aided UAV-RIS Communications," IEEE Access, tập 12, pp. 107971 - 107983, 2024.*

Reconfigurable Intelligent Surfaces for Downlink Cellular Networks

Phuc Quang Truong(✉) and Ca Phan Van

Ho Chi Minh City University of Technology and Education,
Ho Chi Minh City, Vietnam
{phuctq,capv}@hcmute.edu.vn

Abstract. In this work, we propose a joint optimization of power allocation and phase shift for downlink RIS-aided cellular networks. In particular, the total network throughput was maximized under power consumption and QoS constraints. To tackle this problem, we consider power allocation procedure to solve the convex problem of power control coefficients optimization and Block Coordinate Descent (BCD)-based procedure to solve non-convex problem of RIS phase shift optimization. The numerical results are provided to illustrate the effectiveness of the proposed approach in terms of enhancing the coverage and the total network throughput.

Keywords: Reconfigurable intelligent surfaces · Power allocation · Phase shift optimization · Cellular network · Convex optimization

1 Introduction

Reconfigurable Intelligent Surfaces (RISs) are man-made panels that can be capable of configuring the properties of impinging electromagnetic waves based on Snell's law. RIS is the key technology enabling the 6th generation (6G) in the near future. With highlight features, RISs can work without energy source in case of reflecting incident signal only. Different from relaying or decoding and forwarding, RISs can response full-band and nearly not be affected by receiver noise [1]. Due to the potential advantages, RISs are not only the conceptual research but also they are deployed in practical scenarios [2]. The numerical results in [3] prove that RIS-aided wireless communication networks can achieve higher performance than traditional wireless networks.

In [4], the authors assumed the RIS-aided single cell wireless system with multi antennas at the access point (AP) and single antenna at K users. The RIS is equipped with N reflected elements which are controlled by the RIS-controller to switch either receiving mode or reflecting mode. In this case, the total transmit power at the AP is minimized by combining optimizing both active beamforming at the AP and passive beamforming with the user signal-to-interference-plus-noise ratio (SINR) constraints. To tackle this problem, both the semidefinite

Supported by Ho Chi Minh City University of Technology and Education, Vietnam.

N.-S. Vo et al. (Eds.): INISCOM 2022, LNICST 444, pp. 20–32, 2022.
https://doi.org/10.1007/978-3-031-08878-0_2

relaxation (SDR) and alternating optimization algorithms were applied. On the other hand, RIS-aided the wireless network including a base station (BS) with M antennas and K single-antenna users worked in two scenarios: multicasting and multi-user downlink communication. The authors proposed alternating direction method of multipliers (ADMM) algorithm to maximize the smallest signal-to-noise ratio (SNR) in passive beamforming problem [5].

In [6], the authors developed algorithm of low computational complexity to maximize the worst rate subject to the transmit power constraints by jointly designing the reflecting coefficient of RISs and transmit beamformers. In particular, the network of a multiple antenna AP transmitting to multiple single-antenna users, under both proper Gaussian signaling and improper Gaussian signaling with RIS-aided communication in case of without direct link from AP to users.

Recently, RIS-assisted unmanned aerial vehicle (UAV) communication becomes the promising technique to enhance the quality of communication. The scenario in [7] investigated a communication system consisting of a UAV, a ground user, and a RIS on building. Jointly UAV trajectory and passive beamforming at RIS were applied to maximize the average achievable rate of system. Furthermore, the application of UAV becomes more widen in numerous fields such as surveillance, disaster rescue mission, and geography exploration. Hence, the performance network and the quality of service need to enhance and ensure the connection between UAVs and users. In these cases, RIS-assisted multi-UAV networks plays an important role in supporting the connection from UAVs to users when the link is blocked by obstacles. In [8], deep reinforcement learning (DRL) approach was investigated to solve the continuous optimization problem that aimed to maximize the energy efficiency of UAVs networks. Similarly, DRL approach was proposed to maximize the network sum-rate in device-to-device (D2D) communications supported by RIS in [9].

Due to the significant benefits of both spectral efficiency and energy efficiency, non-orthogonal multiple access (NOMA) is the potential technique for future communication networks such as the beyond fifth-generation (B5G), 6G [10]. Thus, the combination of NOMA and RIS will help to enhance the coverage and energy efficiency. Particularly, an RIS-NOMA multi-input-single-output (MISO) system was investigated in [11] to maximize the sum-rate and minimize the total power consumption. To tackle this, the alternating successive convex approximation (SCA) and SDR based algorithms were proposed to solve the jointly transmit beamforming at the BS and passive beamforming at the RIS problems. In [12], the authors assumed that RIS-assisted the wireless power communication network to ensure the connection between a single-antenna BS and single-antenna users. To maximizing the throughput of the network, the authors combined optimizing the reflect beamforming of RIS and the time allocation for power transfer and information transmission BS and users in case of NOMA and time division multiple access (TDMA).

The multi RIS-assisted wireless network including a multi antennas AP and two groups of single antenna users was investigated in [13]. The authors aimed to minimize the transmit power at AP with the individual SINR constraint on information and energy harvesting at energy users.

In [14–16], the authors aimed to maximize the weighted sum rate at all users and the weighted sum power in a RIS-assisted wireless communication system via jointly optimizing the active beamforming at the transmitter and the reflect phase shift at the RISs. Nevertheless, the formulated problems are non-convex. Hence, in [16] the authors based on the fractional programming method to optimize active beamforming at BS and three low-complexity algorithms to solve the passive beamforming problem. Meanwhile, in [14] the authors utilized the sequential rank-one constraint relaxation approach to tackle the passive beamforming problem.

The main contributions of this work focus on extending coverage of the cellular networks by proposing the RIS technology to enhance the reliable of wireless networks, meanwhile the number of users increases rapidly. In particular, to tackle this problem, the joint power allocation at BS and phase shift optimization has been solved by both power allocation procedure in Algorithm 1 and BCD-based procedure in Algorithm 2.

The rest of the paper is organized as follows. We explain the system model of the proposed RIS-assisted downlink cellular network in Sect. 2. Meanwhile, Sect. 3 and Sect. 4 develop the problem statement, methodology and the joint power allocation and phase shift optimization, respectively. The simulation results are discussed in Sect. 5. Finally, the conclusion of the paper is provided in Sect. 6.

2 System Model

2.1 Network Model

In cellular networks, many user equipments (UEs) receive poor signal's quality from the BS because of shadowing and blocking effect. As illustrated in Fig. 1, we study the issue of throughput enhancement for downlink cellular networks with the assistance of RISs panels. Specifically, we assume that the UEs are devided into M groups. And they are uniform randomly distributed in the coverage area. The set of UEs and the group of users are denoted as $\mathcal{K} = \{1, ..., K\}$ and $\mathcal{M} = \{1, ..., M\}$, respectively. The UEs are equipped with a single antenna.

The RISs are installed on the top of buildings, to work as small cell BS where each RIS is consisted of N elements. The m-th group can cover a limited number of UEs, $\mathcal{K}_m = \{1, ..., K_m\}$ for $m \in \mathcal{M}$. The (m, k)-th UE demonstrates the k-th user in the m-th group.

The aim of this paper is to maximize the total throughput of cellular networks by exploiting the RIS technology to extend the coverage of wireless network and to serve many UEs with high QoS.

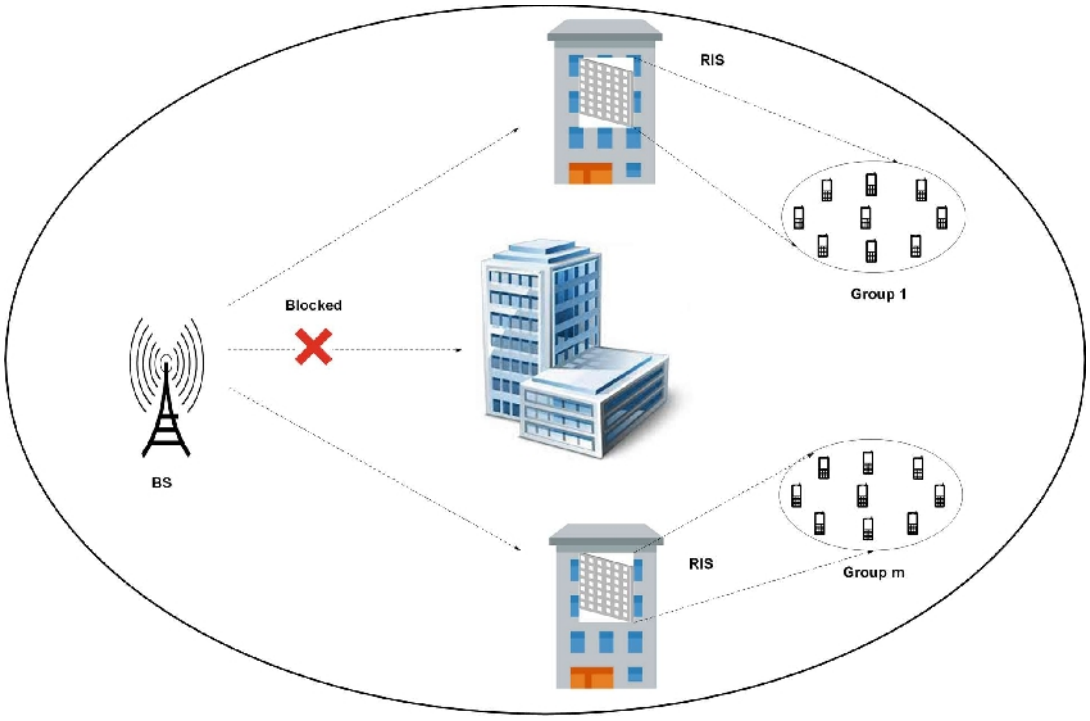

Fig. 1. An illustration of downlink RIS-aided cellular communications.

2.2 RIS-Aided Communication Models

To consider the assistance of RIS in communication models, we investigate the coordinate of the BS, the RISs and of all UEs as (x_0, y_0, H_0), (x_m, y_m, H_m), $m \in \mathcal{M}$ and $(x_k, y_k, 0)$, $k \in \mathcal{K}$, where H_0 and H_m denote the height of the BS and the RIS altitude, respectively.

We focus on enhancing the links between the BS and the RISs. Thus, the path loss of the link from the BS to the m-th RIS follows the free-space path loss, i.e., line of sight (LoS), model as [17,18]

$$\beta_{0,m} = \beta_0 R_{0,m}^{-2}, \ m = 1, ..., M, \tag{1}$$

where we denote β_0 as the channel gain at reference position. In addition, $R_{0,m}$ is the distance between the BS and the m-th RIS, which is give by

$$R_{0,m} = \sqrt{d_{0,m}^2 + (H_0 - H_m)^2}, \tag{2}$$

As mention previous, we assign $d_{0,m} = \sqrt{(x_0 - x_m)^2 + (y_0 - y_m)^2}$.

In contrast, a more complicated non-LoS (NLoS) model is applied to the channel from the RIS to the UEs, which is usually affected by shadowing and blockage geometry. Thus, the path loss of the channel from the m-th RIS to the (m,k)-th UE is formulated as [19]

$$\begin{aligned}\beta_{m,k} &= PL_{m,k} + \eta^{LoS} P_{m,k}^{LoS} + \eta^{NLoS} P_{m,k}^{NLoS} \\ &= 10\alpha \log\left(\sqrt{d_{m,k}^2 + H_{U,m}^2}\right) + AP_{m,k}^{LoS} + B, \end{aligned} \tag{3}$$

where η^{LoS} and η^{NLoS} are the average additional losses for LoS and NLoS, respectively, $A = \eta^{LoS} - \eta^{NLoS}$ and $B = 10\alpha \log(\frac{4\pi f_c R_{m,k}}{c}) + \eta^{NLoS}$. The distance path loss is given by

$$PL_{m,k} = 10 \log(\frac{4\pi f_c R_{m,k}}{c})^{\alpha}, \tag{4}$$

We denote f_c and c as carrier frequency in Hz and the speed of light in m/s, respectively. Where $\alpha \geq 2$ is the path loss exponent. The probability of LoS and NLoS is given by [20]

$$P_{m,k}^{LoS} = \frac{1}{1 + a \exp\left[-b\left(\arctan\left(\frac{H_{U,m}}{d_{m,k}}\right) - a\right)\right]}, \tag{5}$$

$$P_{m,k}^{NLoS} = 1 - P_{m,k}^{LoS}, \tag{6}$$

where both a and b are the constants of the environment.

Furthermore, we consider the effect of the phase shift matrix at the m-th RIS $\mathbf{\Phi}_m = diag[\phi_{1m}, \phi_{2m}, ..., \phi_{Nm}]$, here $\phi_{nm} = \alpha_{nm} e^{j\theta_{nm}}$ with $\alpha_{nm} \in [0,1]$ and $\theta_{nm} \in [0, 2\pi]$ $(\forall n = 1, 2, ..., N,\ m \in \mathcal{M})$, that indicates the amplitude of the reflected signal and phase shift of the n-th reflecting element, respectively. We assign $\alpha_{nm} = 1$ because the reflecting element can not change the amplitude of reflecting signals [21]. Under this effect, the small scale fading coefficients, which are assumed as independent and identically distributed random variables with zero mean and unit variance, are used for the link from the BS to m-th RIS and the m-th RIS to the (m,k)-th UE, indicated by $\hat{h}_{0,m} \in \mathbb{C}^{N \times 1}$ and $\hat{h}_{m,k}^H \in \mathbb{C}^{1 \times N}$, respectively. The H is the Hermitian conjugate operation.

Additionally, we denote $\mathbf{h}_{0,m} \in \mathbb{C}^{N \times 1}$ and $\mathbf{h}_{m,k}^H \in \mathbb{C}^{1 \times N}$ as the channel matrix between the BS and the m-th RIS and the m-th RIS to the (m,k)-th UE in the m-th group, respectively. Nevertheless, the cascaded channel matrix of the link between the BS and the (m,k)-th UE through the m-th RIS, $\mathbf{g}_{m,k} \in \mathbb{C}$, can be rewritten as [22]

$$\mathbf{g}_{m,k} = \mathbf{h}_{m,k}^H \mathbf{\Phi}_m \mathbf{h}_{0,m}, \tag{7}$$

where $\mathbf{h}_{0,m} = \sqrt{\beta_{0,m}} \hat{h}_{0,m}$ and $\mathbf{h}_{m,k}^H = \sqrt{\beta_{m,k}} \hat{h}_{m,k}^H$.

2.3 Transmission Schemes

As shown in Fig. 1, the BS transmits signal to its UEs with the reflection from RIS panel deployed on the top of buildings. With TDMA scheme, we have the signal at the k-th UE in the m-th group below

$$y_{m,k} = \sqrt{p_{m,k}}\mathbf{g}_{m,k}s_{m,k} + \ n_k, \tag{8}$$

where $p_{m,k}$ is the transmission power of the BS to the (m,k)-th UE; $s_{m,k}$ is information transmitted by the BS such that $||s_{m,k}||^2 \leq 1$; $n_k \sim \mathcal{CN}(0, \sigma_k^2)$ is the AWGN at the (m,k)-th UE.

Let $\boldsymbol{p}_0 = [\boldsymbol{p}_{0,m}]_{m=1}^{M}$, here $\boldsymbol{p}_{0,m} = [p_{m,k}]_{k=1}^{K_m}$, and $\boldsymbol{\Phi}_M = [\boldsymbol{\Phi}_m]_{m=1}^{M}$ denote the power control coefficients and the phase shifts of RISs, respectively, the received SNR at the (m,k)-th UE can be formulated as

$$\gamma_{m,k}\left(p_{m,k}, \boldsymbol{\Phi}_m\right) = \frac{p_{m,k}\left|\mathbf{g}_{m,k}\right|^2}{\sigma_k^2}. \tag{9}$$

2.4 Information Throughput

The information throughput of the (m,k)-th UE (in bps/Hz) can be expressed as

$$R_{m,k}\left(p_{m,k}, \boldsymbol{\Phi}_m\right) = \log_2\left(1 + \gamma_{m,k}\left(p_{m,k}, \boldsymbol{\Phi}_m\right)\right). \tag{10}$$

Hence, the total throughput of all the UEs in the network can be given by

$$R_{total}\left(\boldsymbol{p}_0, \boldsymbol{\Phi}_M\right) = \sum_{m=1}^{M}\sum_{k=1}^{K_m} R_{m,k}\left(p_{m,k}, \boldsymbol{\Phi}_m\right). \tag{11}$$

3 Problem Statement and Methodology

In this paper, we focus on maximizing the total throughput of downlink cellular networks. To tackle this problem, we jointly optimize $(\boldsymbol{p}_0)$ at the BS and $(\boldsymbol{\Phi}_M)$ of M RISs given some power consumption and QoS constraints. The corresponding optimization problem is as follows:

$$\max_{\boldsymbol{p}_0, \boldsymbol{\Phi}_M} \ R_{total}\left(\boldsymbol{p}_0, \Phi_M\right) \tag{12a}$$

$$\text{s.t.} \quad \sum_{m=1}^{M}\sum_{k=1}^{K_m} p_{m,k} \leq P_0^{\max}, m \in \mathcal{M}, \tag{12b}$$

$$R_{m,k}\left(p_{m,k}, \boldsymbol{\Phi}_m\right) \geq \bar{r}_{m,k}, \ m \in \mathcal{M}, \ k \in \mathcal{K}_m, \tag{12c}$$

$$0 \leq \theta_{nm} \leq 2\pi, \forall n = 1, 2, ..., N, \ m \in \mathcal{M}, \tag{12d}$$

where (12b) is used to limit the total power consumption of all RISs not greater than the maximum transmit power of the BS $(P_0^{\max})$. Meanwhile, (12c) is the QoS constraint at the (m,k)-th UE. And (12d) indicates the lower and upper bounds of the phase shifts when considering the n-th reflecting element of the m-th RIS.

4 Joint Power Allocation and Phase Shift Optimization

It is obvious that the problem (12) is non-convex with the non-convex functions of (12a) and (12c). Therefore, we iteratively optimize the power control coefficients of the BS and the phase shifts of RIS reflecting elements.

4.1 Power Control Coefficients Optimization

For any given $\mathbf{\Phi}_M$, (12) is equivalent to the following power control coefficients optimization problem

$$\max_{\boldsymbol{p}_0} R_{total}\left(\boldsymbol{p}_0\right) \tag{13a}$$

$$\text{s.t.} \quad (12b), (12c). \tag{13b}$$

To solve (13), we utilize the effective approximations and logarithm inequalities [23] based on the property of the convex function $f(z) = \log_2(1+\frac{1}{z}) \geq \hat{f}(z)$, where

$$\hat{f}(z) = \log_2\left(1+\frac{1}{\overline{z}}\right) + \frac{1}{1+\overline{z}} - \frac{z}{(1+\overline{z})\overline{z}}, \tag{14}$$

$\forall z > 0, \overline{z} > 0$. Then, we can write

$$R_{m,k}\left(p_{m,k}\right) \geq \hat{R}^{(i)}_{m,k}\left(p_{m,k}\right), \ \forall k \in \mathcal{K}_m, \ \forall m \in \mathcal{M}, \tag{15}$$

where

$$z = \frac{\sigma_k^2}{p_{m,k}\left|\boldsymbol{g}_{m,k}\right|^2}, \ \overline{z} = z^{(i)} = \frac{\sigma_k^2}{p^{(i)}_{m,k}\left|\boldsymbol{g}_{m,k}\right|^2},$$

$$\hat{R}^{(i)}_{m,k}\left(p_{m,k}\right) = \log_2\left(1+\frac{1}{\overline{z}}\right) + \frac{1}{1+\overline{z}} - \frac{z}{(1+\overline{z})\overline{z}}. \tag{16}$$

So far, (13) can be rewritten as (17) to yield the feasible points at the i-th iteration:

$$\max_{\boldsymbol{p}_0} \hat{R}^{(i)}_{total}\left(\boldsymbol{p}_0\right) \tag{17a}$$

$$\text{s.t.} \quad (12b), \tag{17b}$$

$$\hat{R}^{(i)}_{m,k}\left(\boldsymbol{p}_0\right) \geq \overline{r}_{m,k}, \ m \in \mathcal{M}, \ k \in \mathcal{K}_m, \tag{17c}$$

where $\hat{R}^{(\kappa)}_{total}\left(\boldsymbol{p}_0\right) = \sum_{m=1}^{M}\sum_{k=1}^{K_m}\hat{R}^{(\kappa)}_{m,k}\left(p_{m,k}\right)$.

Finally, we solve (17) by CVX tools [24] following the Algorithm 1. Particularly, we set up the values of $i = 0$, $\mathbf{\Phi}_M$, and $\varepsilon = 10^{-3}$. The number of iterations is $I_{max} = 20$. The output is the optimal power control coefficients $(\boldsymbol{p}_0^*)$.

Algorithm 1. Power allocation procedure

Input:
$i = 0$, $\boldsymbol{\Phi}_M$, $\varepsilon = 10^{-3}$
$I_{max} = 20$
while (Divergence or $i \leqslant I_{max}$)
Solve (17) for ($\boldsymbol{p}_0^{(i+1)}$) by CVX
$i = i + 1$
end while
Output: $\boldsymbol{p}_0^*$

4.2 RIS Phase Shift Optimization

With the considering power control coefficients $\boldsymbol{p}_0$, the problem can be rewritten as

$$\max_{\boldsymbol{\Phi}_M} R_{total}\left(\boldsymbol{\Phi}_M\right) \tag{18a}$$

$$\text{s.t.} \quad (12c), (12d). \tag{18b}$$

Let $\boldsymbol{h}_{m,k}^H \boldsymbol{\Phi}_m \boldsymbol{h}_{0,m} = \psi_m^H \chi_{m,k}$ where $\psi_m = [\psi_m^1, ..., \psi_m^N]^H$ with $\psi_m^n = e^{j\theta_{nm}}$ ($\forall n = 1, 2, ..., N$), $\chi_{m,k} = diag(\boldsymbol{h}_{m,k}^H)\boldsymbol{h}_{0,m}$, and $a_k = P_0/\sigma_k^2$. With $|\psi_m^n|^2 = 1$, the constraint in (12d) becomes the unit-modulus constraint [4]. Then, the problem (18) is equivalently rewritten as

$$\max_{\psi_m,\ m\in\mathcal{M}} \sum_{m=1}^{M}\sum_{k=1}^{K_m} \log_2\left(1 + a_k \psi_m^H \chi_{m,k} \chi_{m,k}^H \psi_m\right) \tag{19a}$$

$$\text{s.t.} \quad \psi_m^H \chi_{m,k} \chi_{m,k}^H \psi_m \geq \left(2^{\bar{r}_{m,k}} - 1\right)/a_k, \tag{19b}$$

$$|\psi_m^n|^2 = 1, \forall n = 1, 2, ..., N,\ m \in \mathcal{M}. \tag{19c}$$

Nevertheless, (19) is non-convex. To make (19) become a convex optimization problem, we first denote $\mathbf{X}_{m,k} = \chi_{m,k}\chi_{m,k}^H$ and $\psi_m^H \mathbf{X}_{m,k} \psi_m = tr\left(\mathbf{X}_{m,k}\psi_m\psi_m^H\right) = tr\left(\mathbf{X}_{m,k}\boldsymbol{\Psi}_m\right)$ where $\boldsymbol{\Psi}_m = \psi_m\psi_m^H$ must satisfy $\boldsymbol{\Psi}_m \succeq \mathbf{0}$ and rank($\boldsymbol{\Psi}_m$)=1. And then, we relax the rank-one constraint of (19c) [6]. Thus, (19) is rewritten as

$$\max_{\psi_m,\ m\in\mathcal{M}} \sum_{m=1}^{M}\sum_{k=1}^{K_m} \log_2\left(1 + a_k tr\left(\mathbf{X}_{m,k}\boldsymbol{\Psi}_m\right)\right) \tag{20a}$$

$$\text{s.t.} \quad tr\left(\mathbf{X}_{m,k}\boldsymbol{\Psi}_m\right) \geq \left(2^{\bar{r}_{m,k}} - 1\right)/a_k, \tag{20b}$$

$$\boldsymbol{\Psi}_{m(n,n)} = 1, \forall n = 1, 2, ..., N,\ m \in \mathcal{M}, \tag{20c}$$

$$\boldsymbol{\Psi}_m \succeq \mathbf{0}. \tag{20d}$$

As a result, we can see that problem (20) is a convex semidefinite program (SDP) [4], which can be efficiently solved by using CVX. We proposed BCD-based method to solve problem (20) in Algorithm 2. Specifically, we assign $i = 0$,

$\boldsymbol{p}_0$, $\boldsymbol{f}_{m,k}^{(0)}$, and $\varepsilon = 10^{-3}$. The output of this algorithm is the optimal phase shift $(\boldsymbol{\Phi}_M^*)$.

Algorithm 2. Phase shift searching procedure

Input:
$i = 0$, $\boldsymbol{p}_0$, $\boldsymbol{f}_{m,k}^{(0)}$, $\varepsilon = 10^{-3}$
$I_{max} = 20$
while (Divergence or $i \leqslant I_{max}$)
for $m = [1 : M]$
Solve (20) for $(\boldsymbol{\Phi}_M^{(i+1)})$ by CVX
$\boldsymbol{f}_{m,k}^{(i+1)}$
end for
$i = i + 1$
end while
Output: $\boldsymbol{\Phi}_M^*$

Lastly, the Algorithms 1 and 2 are combined to solve the joint power allocation and phase shifts optimization.

5 Simulation Results

In this section, we investigate simulation results in Matlab to figure out the performance of the proposed method. We consider parameters of simulation as follows. The radius of circle coverage is 500 m. The radius of expanded deployment area is 2000m. In additional, we assume that the BS is located at $(0, 0, 30)$. The white power spectral density and QoS threshold are assigned to $\sigma^2 = -130$ dBm/Hz and $\bar{r}_{m,k} = 1$ bps/Hz, respectively. In term of the channel model, we set up the same as the settings in [23,25]. We conduct numerical results from our proposed method as in (12) i.e., optimal power allocation - optimal phase shift (OP-OPH), and the conventional methods i.e., optimal power allocation - random phase shift (OP-RPH), equal power allocation - random phase shift (EP-OPH), and equal power allocation - random phase shift (EP-RPH).

In Fig. 2 and Fig. 3, the total network throughput is plotted in two scenarios with the number of reflecting elements is fixed $N = 50$. In Fig. 2, we assume that the number of RISs and the number of UEs are $M = 4$ and $K = 20$, respectively. The number RISs is $M = 8$ and the number of UEs is $K = 30$ in Fig. 3. It is clear that the total network throughput rises when the transmit power at the BS increases. Specifically, when the number of RISs is increased, the total network throughput rises considerably. Moreover, in the consider method, the optimal phase shift can be more efficient than the others in all scenarios in Fig. 2 and Fig. 3.

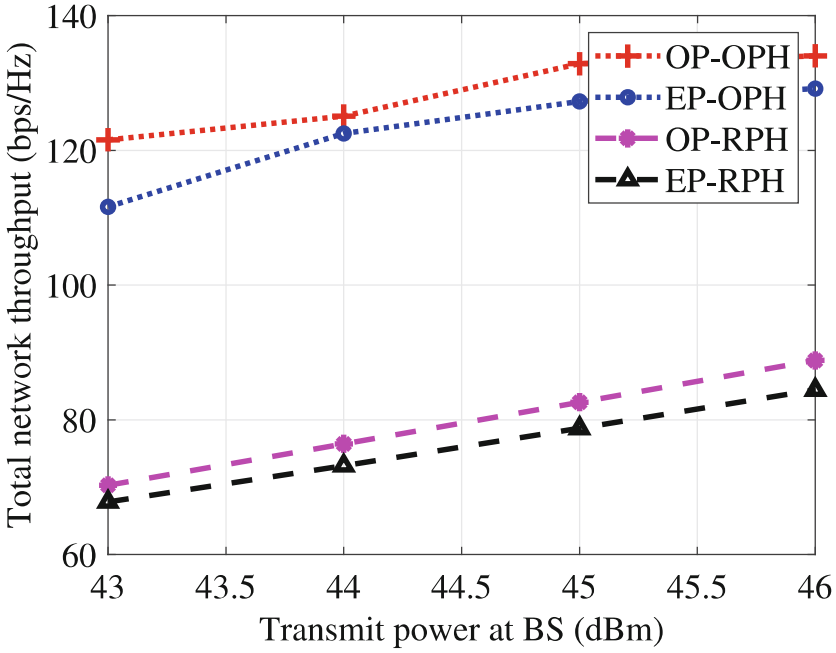

Fig. 2. Total throughput versus number of RISs ($M = 4$, $K = 20$, $N = 50$).

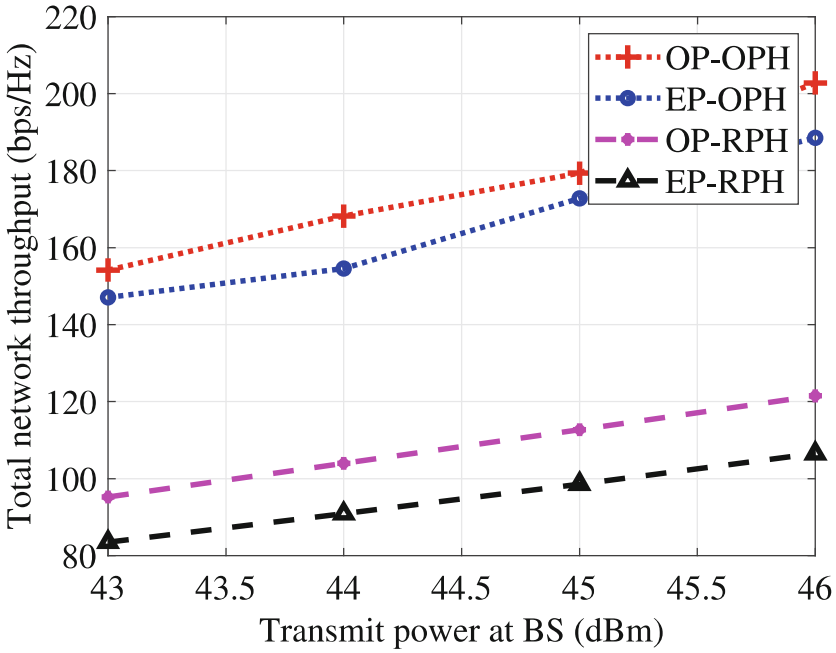

Fig. 3. Total throughput versus transmission power at BS ($M = 8$, $K = 30$, $N = 50$).

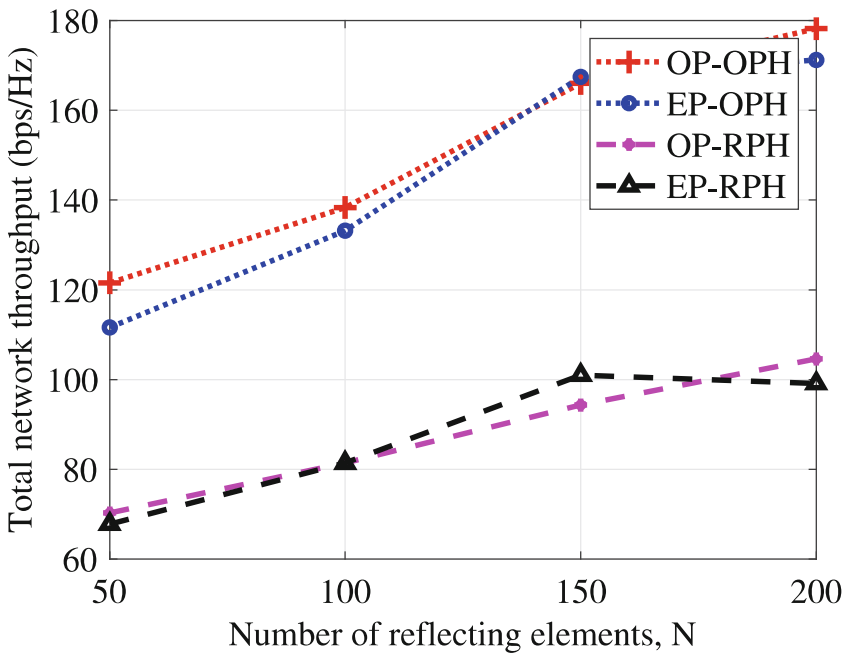

Fig. 4. Total throughput versus number of reflecting elements ($M = 4$, $K = 20$, $P_0^{\max} = 43$ dBm).

Meanwhile, we illustrate the total network throughput versus different of RIS elements when $M = 4$, $K = 20$, and $P_0^{\max} = 43$ dBm in Fig. 4. Clearly, as can be seen that the total network throughput grows steadily when the number of reflecting elements rises. In particular, the result shows that the total network throughput of proposed network is significantly larger than others in case the phase shift is optimized. As expected, the OP-OPH is the best method for RIS-aided downlink cellular network. Despite the fact that $P_0^{\max}$ is fixed to 43 dBm, the OP-OPH method can achieve approximately much more 1,8 times than the EP-RPH method.

Finally, in case of the number of RIS $M = 4$, the number of user $K = 20$, and $P_0^{\max} = 43$ dBm, the results in Fig. 2 and Fig. 4 prove that the total network throughput heightens about 1,5 times when we increase the number of reflecting elements from $N = 50$ to $N = 200$.

6 Conclusions

In this paper, we have studied the assistance of RIS for downlink cellular networks. Aiming to enhance the QoS of cellular network, the joint power allocation coefficients of BS and phase shifts of RIS optimization was applied. The numerical results demonstrated the efficiency of proposed system. The total network throughput achieved the highest in case both power and phase shift are optimized. Obviously, the coverage is expanded thanks to the RIS assisted, but not investigated in this paper.

References

1. Basar, E., Di Renzo, M., De Rosny, J., Debbah, M., Alouini, M.-S., Zhang, R.: Wireless communications through reconfigurable intelligent surfaces. IEEE Access **7**, 116753–116773 (2019)
2. Wu, Q., Zhang, S., Zheng, B., You, C., Zhang, R.: Intelligent reflecting surface-aided wireless communications: a tutorial. IEEE Trans. Commun. **69**(5), 3313–3351 (2021)
3. Wu, Q., Zhang, R.: Towards smart and reconfigurable environment: intelligent reflecting surface aided wireless network. IEEE Commun. Mag. **58**(1), 106–112 (2020)
4. Wu, Q., Zhang, R.: Intelligent reflecting surface enhanced wireless network via joint active and passive beamforming. IEEE Trans. Wireless Commun. **18**(11), 5394–5409 (2019)
5. Huang, K.-W., Wang, H.-M.: Passive beamforming for IRS aided wireless networks. IEEE Wireless Commun. Lett. **9**(12), 2035–2039 (2020)
6. Yu, H., Tuan, H.D., Nasir, A.A., Duong, T.Q., Poor, H.V.: Joint design of reconfigurable intelligent surfaces and transmit beamforming under proper and improper gaussian signaling. IEEE J. Sel. Areas Commun. **38**(11), 2589–2603 (2020)
7. Li, S., Duo, B., Yuan, X., Liang, Y.-C., Di Renzo, M.: Reconfigurable intelligent surface assisted UAV communication: joint trajectory design and passive beamforming. IEEE Wireless Commun. Lett. **9**(5), 716–720 (2020)
8. Nguyen, K.K., Khosravirad, S., da Costa, D.B., Nguyen, L.D., Duong, T.Q.: Reconfigurable Intelligent Surface-assisted Multi-UAV Networks: Efficient Resource Allocation with Deep Reinforcement Learning (2021)
9. Nguyen, K.K., Masaracchia, A., Yin, C., Nguyen, L.D., Dobre, O.A., Duong, T.Q.: Deep Reinforcement Learning for Intelligent Reflecting Surface-Assisted D2D Communications (2021)
10. Ha, D.-B., Truong, V.-T., Lee, Y.: Performance analysis for RF energy harvesting mobile edge computing networks with SIMO/MISO-NOMA schemes. EAI Endorsed Trans. Ind. Netw. Intell. Syst. **8**(27), 4 (2021)
11. Fang, F., Xu, Y., Pham, Q.-V., Ding, Z.: Energy-efficient design of IRS-NOMA networks. IEEE Trans. Veh. Technol. **69**(11), 14088–14092 (2020)
12. Zhang, D., Wu, Q., Cui, M., Zhang, G., Niyato, D.: Throughput maximization for IRS-assisted wireless powered hybrid NOMA and TDMA. IEEE Wireless Commun. Lett. **10**(9), 1944–1948 (2021)
13. Wu, Q., Zhang, R.: Joint active and passive beamforming optimization for intelligent reflecting surface assisted SWIPT under QoS constraints. IEEE J. Sel. Areas Commun. **38**(8), 1735–1748 (2020)
14. Mu, X., Liu, Y., Guo, L., Lin, J., Al-Dhahir, N.: Exploiting intelligent reflecting surfaces in NOMA networks: joint beamforming optimization. IEEE Trans. Wireless Commun. **19**(10), 6884–6898 (2020)
15. Wu, Q., Zhang, R.: Weighted sum power maximization for intelligent reflecting surface aided SWIPT. IEEE Wireless Commun. Lett. **9**(5), 586–590 (2020)
16. Guo, H., Liang, Y.-C., Chen, J., Larsson, E.G.: Weighted sum-rate maximization for intelligent reflecting surface enhanced wireless networks. In: IEEE Global Communications Conference (GLOBECOM) 2019, pp. 1–6 (2019)
17. Nguyen, M., Nguyen, L.D., Duong, T.Q., Tuan, H.D.: Real-time optimal resource allocation for embedded UAV communication systems. IEEE Wireless Commun. Lett. **8**(1), 225–228 (2019)

18. Bor-Yaliniz, R.I., El-Keyi, A., Yanikomeroglu, H.: Efficient 3-D placement of an aerial base station in next generation cellular networks. In: IEEE ICC, pp. 1–5, May 2016
19. Mozaffari, M., Saad, W., Bennis, M., Debbah, M.: Efficient deployment of multiple unmanned aerial vehicles for optimal wireless coverage. IEEE Commun. Lett. **20**, 1647–1650 (2016)
20. Al-Hourani, A., Kandeepan, S., Lardner, S.: Optimal LAP altitude for maximum coverage. IEEE Wireless Commun. Lett. **3**(6), 569–572 (2014)
21. Xie, X., Fang, F., Ding, Z.: Joint optimization of beamforming, phase-shifting and power allocation in a multi-cluster IRS-NOMA network. IEEE Trans. Veh. Technol. **70**(8), 7705–7717 (2021)
22. Wu, Q., Zhang, R.: Beamforming optimization for wireless network aided by intelligent reflecting surface with discrete phase shifts. IEEE Trans. Commun. **68**(3), 1838–1851 (2020)
23. Nguyen, L.D., Tuan, H.D., Duong, T.Q., Dobre, O.A., Poor, H.V.: Downlink beamforming for energy-efficient heterogeneous networks with massive MIMO and small cells. IEEE Trans. Wireless Commun. **17**(5), 3386–3400 (2018)
24. Grant, M., Boyd, S.: CVX: MATLAB software for disciplined convex programming, version 2.1, March 2014. http://cvxr.com/cvx
25. Do-Duy, T., Nguyen, L.D., Duong, T.Q., Khosravirad, S., Claussen, H.: Joint optimisation of real-time deployment and resource allocation for UAV-aided disaster emergency communications. IEEE J. Sel. Areas Commun. **39**(11), 3411–3424 (2021)

EAI Endorsed Transactions
Industrial Networks and Intelligent Systems
Research Article EAI.EU

Jointly power allocation and phase shift optimization for RIS empowered downlink cellular networks

Phuc Quang Truong[1,*], Tan Do-Duy[1], Van-Ca Phan[1], and Antonino Masaracchia[2]

[1]Faculty of Electrical and Electronics Engineering, Ho Chi Minh City University of Technology and Education
No.1, Vo Van Ngan street, Thu Duc City, Ho Chi Minh City, Vietnam
[2]School of Electronics, Electrical Engineering, and Computer Science, Queen's University Belfast,
Belfast BT7, 1NN, UK

Abstract

Reconfigurable Intelligent Surfaces (RIS) have been highlighted by the research community as a key enabling technology for the enhancement of next-generation wireless network performance, including energy efficiency, spectral efficiency, and network throughput. This paper investigates how RIS-assisted communication can effectively maximize the downlink throughput of a cellular network. Specifically, the paper considers a communication scenario where a single base station serves multiple ground users with the aid of an RIS placed on a building facade. For such a communication scenario, we considered an optimization problem aimed at maximizing the overall downlink throughput by jointly optimizing power allocation at the base station and phase shift of RIS reflecting elements, subject to power consumption and quality-of-service constraints. To address its non-convex nature, the original optimization problem has been divided into two subproblems. The first one, for power control with fixed phase shift values, is a convex problem that can be easily solved. Subsequently, a phase shift searching procedure to solve the non-convex problem of RIS phase shift optimization has been adopted. The results from numerical simulations show that the proposed method outperforms other conventional methods proposed in the literature. In addition, computational complexity analysis has been conducted to prove the low complexity of the proposed method.

Keywords: 6G, Optimization, Phase-Shift Optimization, QoS, Resource Allocation, RIS, Throughput Maximization

Received on 10 November 2023; accepted on 07 December 2023; published on 11 December 2023

doi:10.4108/eetinis.v10i4.4359

1. Introduction

The current generation of wireless communication systems is experiencing a huge increase of connected mobile devices with a corresponding exponential increase of mobile data traffic. According to data analysis and forecasts from the International Telecommunication Union Radiocommunication Sector (ITU-R), this trend will inevitably cause a collapse of the current 5G networks in the near future [2]. Under these perspectives, both industry and academia are actively working towards the development of the new wireless communication network referred as sixth-generation (6G). This new standard is expected to introduce innovative physical layer technologies that, compared to 5G, will provide increased network capacity, as well as increased reduced latency and better communication reliability [3–5]. Reconfigurable intelligent surface (RIS) is one of these potential technology for 6G [6]. More specifically, RIS is a two-dimensional surface consisting of massive reflecting elements, which are entirely programmable through the usage of appropriate external signals [7]. As result, the adoption of RIS will allow to reflect and redirect the transmitted signal enabling then the possibility to control the signal propagation over the wireless medium. As illustrated in Figure 1, through a RIS-enabled communication scenario it results possible to manipulate and reflect radio signals in order to ensure improved coverage and signal quality, even in

*Corresponding author. Email: phuctq@hcmute.edu.vn
This article was presented in part at International Conference on Industrial Networks and Intelligent Systems (INISCOM), 2022 [1].

challenging environments. Furthermore, compared to massive multiple-input multiple-output (MIMO) technology, RIS represents a more cost-effective and energy-efficient solution. [8]. As result, the adoption of RIS in wireless communication scenarios has gathered significant attention from the research community, who have recognized it as a pivotal enabling technology for 6G due to its immense potential and capabilities [9]. Some of the most relevant works are discussed in the next subsection.

1.1. Related works on RIS

Authors in [10] proved how, compared to amplify-and-forward (AF), a RIS-assisted wireless communication system outperforms in terms of ergodic capacity (EC)and outage probability, and then in terms of lower symbol error rate (SER) and average end-to-end signal-to-noise ratio (SNR). Particularly, the end-to-end wireless channel from source to destination with the assistance of single RIS and multiple RISs was considered, then, the authors derived the close-form expression for OP, and SER in both investigate cases. Likewise, the close-form expression of instantaneous, average end-to-end SNR, and EC of both RIS-assisted RF-relaying wireless system are derived to analyze the performance in case of single RIS and multi-RISs. Additionally, in [11] they considered communication scenario with single antenna at both transmitter and receiver, assisted by a RIS with N reflecting elements. In order to validate the performances of such RIS-asssited scenario, they provided a closed-form expressions the EC upper bound and outage probability approximation under the assumption of mixed Rayleigh and Rician fading channels, which have been validated by using Monte Carlo simulations. This has been further validated in [12], by deriving closed-form expressions for the OP, average SER and average communication rate. Last but not least, the authors also shown how the number of reflecting elements of RIS in single-input single-output (SISO) channel impact on channel diversity. A RIS-aided SISO wireless system with underlying non-orthogonal multiple access (NOMA) communication consisting has been considered in [13]. In this case, OP of the considered system has been derived in closed-form, showing the significant benefit of RIS in enhancing the coverage under the new channel statistics link from BS to cell-edge user devices via RIS with Nakagami-m fading.

In addition to the mathematical models that represents a tangible tool for demonstrating the potential of RIS-assisted communications, several studies have also been conducted with the main aim of optimizing the main variables of the entire communication system and then maximizing the overall system performances. An optimization framework aimed at maximizing the energy efficiency (EE) of a multiple-input single-output (MISO) RIS-assisted network was proposed in [14]. The proposed optimization framework jointly optimized power allocation at the base station and the phase shift of the RIS to serve multiple users.

Optimization strategies to maximize the weighted sum rate (WSR) of all users have been proposed in [15, 16]. More specifically, authors in [15] considered an RIS-assisted multi-user MISO wireless communication scenario. The considered system consisted in an N-element RIS and one multi-antenna wireless access point providing services to single-antenna users in a quasi-static flat-fading channel environment. In this context, WSR of the network was maximized by jointly optimizing beamforming at the access point and RIS phase-shoft vector. On the other hand, a RIS-aided millimetre-wave (mmWave) massive MIMO was considered in [16]. More specifically, authors considered a system where the direct links between the BS and mobile users are blocked by objects. Under this assumptions, the WSR was maximized by jointly optimizing BS's beamforming matrix and the RIS's phase-shift vector.

An iterative optimization algorithm to maximize the achievable rate of a MIMO system equipped with a RIS have been proposed in [17]. In this case, the proposed algorithm jointly optimized the covariance matrix of the transmitted signal and the phase shift coefficients of RIS elements.

Recently, the possibility of including RIS into unmanned aerial vehicle (UAV) communication scenarios has also gaining attention. Indeed, compared to the conventional BS-based communications, the simultaneous usage of these technologies within the same communication area definitively allows for improving the strength f the signal received by the ground users [18–20]. However, these types of communication scenarios comes with additional variables to optimized in order to maximize the entire system performances, especially in particular where an high quality of connection between UAV and ground users must be guaranteed, such as disaster rescue mission and geography exploration.

Authors in [21] considered a communication scenario with a single UAV, a ground user, and an RIS placade on a building facade. For this communication setup, in order to maximize the average achievable system rate, an optimization framework that jointly optimizes the beamforming vector and the UAV's trajectory was proposed.

In [22], a deep reinforcement learning (DRL) based approach was investigated to maximize the EE of multi-UAV networks. To tackle this problem, a DRL-based method the joint optimization of RIS phase shift optimization and power allocation of UAVs was proposed and validated.

The problem of maximizing the average achievable rate of a RIS-aided UAV network was presented in [23]. To deal with the non-convexity of such problem, the authors proposed to divide the original problem into two sub-problems, i.e., one for passive beamforming optimization and anther for trajectory optimization. Nevertheless, the main focus in [24] was on the maximization of total network throughput through the optimization power allocation and phase shift subject to power consumption constraints and minimum guaranteed quality-of-service at users.

The usage of RIS technology is also gaining attention in the context of Mobile Edge Computing (MEC) scenarios. The usage of RIS within a MEC scenario holds the potential to address the latency requirements envisioned for 6G-enabled MEC services. Especially, in [25] proposed the RIS-aided NOMA network combined with radio frequency energy harvesting and MEC technique. To evaluate the effectiveness of networks parameters to the proposed scheme, the authors considered the optimization problem with two object functions including the probabilities of task offloading and energy transfer efficiency. It is worth to mention that in RIS-aided MEC system, the radio, computing, and wireless environment are considered to optimize [26, 27]. In line with this view, the objective in [26] is to optimize resource allocation including the transmit power and the computing capacity of the RIS-assisted MEC system. It is highlighted that the authors formulated the RIS optimization problem for dependent RIS response profiles over the multi-carrier frequency selective channels. Meanwhile, to overcome the huge challenges of wireless network including the limited coverage and computational capacity, the authors propose the UAV-RIS assisted MEC network in [27]. To exploit the potential of proposed scheme, the authors derived the max-min computation capacity problem through considering the trajectory, computation capacity, beamforming of UAV, and time slot partition, uplink signal detection, and beamforming at RIS as well.

1.2. Motivation and Contributions

This paper represents an extension of the work resented in [1]. In particular, we extend our previous work by jointly optimizing the phase-shift matrix at RIS and power allocation at BS subject to minimum quality-of-service and power constraints, showing how the performances varies as the number of RISs in the area increases. Then, the main contributions of this work can be summarized as follow: The main contributions of this paper are listed as follows:

- We consider a RIS-aided wireless communication scenario were different RISs are deployed in order to provide downlink service to group of users. For such scenario we formulated an optimization problem aimed at maximizing the total network throughput under the power consumption and quality-of-service constraints.

- Due to the non-convexity nature of the proposed problem, we divided into two sub-problems, for which an iterative frameworks is proposed. Such framework summarized in Algorithm 1 and Algorithm 2, was based on the usage of effective approximations, logarithm inequalities for relaxation.

- Finally, we investigated how the proposed joint optimization method outperform in maximizing total network throughput and the worst case mobile unit throughput compared to conventional methods.

The rest of the paper is organized as follows. System model and the problem formulation are provided in Section 2.1. Section 3, illustrates the joint power allocation and phase shift optimization, and how it is divided into two subproblems including power control coefficients optimization and RIS phase shift optimization, respectively. Simulation and performance evaluations results are discussed in Section 4. Finally, the paper is concluded Section 5.

Table 1. Notations

Symbol	Definition
H_0, H_m	BS and the RIS height, respectively.
$\mathbf{\Phi}_m$	Phase shift matrix of the m-th RIS
H	Hermitian conjugate operation
$\mathbf{h}_{0,m} \in \mathbb{C}^{N\times 1}$	Channel matrix between the BS and the m-th RIS
$\mathbf{h}_{m,k}^H \in \mathbb{C}^{1\times N}$	Channel matrix between the m-th RIS to the (m, k)-th MU
$p_{m,k}$	Transmission power of BS to the (m,k)-th MU
$\omega_k \sim \mathcal{CN}(0,\sigma_k^2)$	AWGN at the (m,k)-th MU
α	Path loss exponent
$\mathbf{g}_{m,k} \in \mathbb{C}$	Cascaded channel matrix of the link BS-(m,k)th MU
$p_{m,k}$	Transmission power of the BS to the (m,k)-th MU
η^{LoS}, η^{NLoS}	Average additional losses of LoS and NLoS

2. System Model and Problem Formulation

In this section, we investigate the signal model for downlink multi-user SISO cellular network, then we formulate an optimization problem for maximizing the total network throughput by jointly optimal allocation of of transmit power at BS and phase shift of RIS.

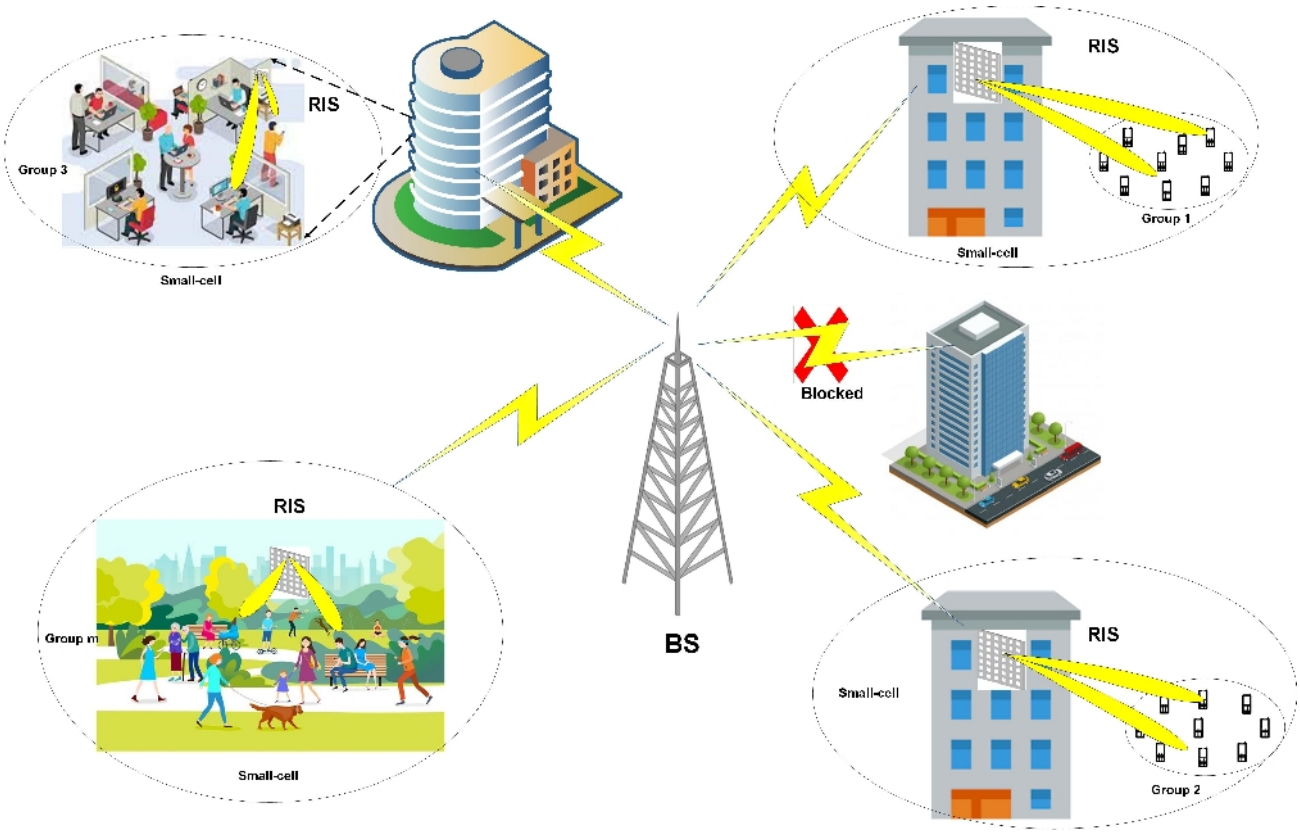

Figure 1. RIS-assisted downlink cellular communications.

2.1. System Model

Due to the objects obstructing the communication link, the mobile users (MUs) in cellular network either receive low quality signal or not signal at all from the BS. To tackle this problem, we propose the system model in Fig. 1, particularly we focus on enhancing the total network throughput of the multi-user cellular network with the assistance of RISs. More specifically, how illustrated in Fig. 1, we consider a single antenna BS serving a set of $\mathcal{M} = \{1, ..., M\}$ small cells, each of them containing different numbers of MUs, which are supposed to be uniformly distributed within the whole coverage area. All these aures are indicated as $\mathcal{K} = \{1, ..., K\}$. In order to solve the issue by blockage effect from buildings and other obstacles, it is supposed that different N-elemment RISs are placed on the facade of different buildings building, each of them used to cover a specific small cell. The number of MUs covered by the m-th cell are indicated as $\mathcal{K}_m = \{1, ..., K_m\}$ for $m \in \mathcal{M}$, while the k-th user within the m-th group as (m, k)

2.2. Communication Model

Within the considered communication scenario, the 3D Cartesian coordinates of the BS, the RISs and of the generic MU are indicated as (x_0, y_0, H_0), (x_m, y_m, H_m), $m \in \mathcal{M}$ and $(x_k, y_k, 0)$, $k \in \mathcal{K}$, with H_0 and H_m being the z-coordinate, i.e., height the BS and the RIS altitude, respectively. We assume that there exists a direct communication between BS and the m-th RIS. Then, as also assumed in [28, 29], such communication link follow the free-space path loss model:

$$\beta_{0,m} = \beta_0 l_{0,m}^{-2}, \ m = 1, ..., M, \tag{1}$$

with β_0 being the channel gain at reference position, and $l_{0,m}$ the distance between the BS and the m-th RIS calculated as:

$$l_{0,m} = \sqrt{d_{0,m}^2 + (H_0 - H_m)^2}, \tag{2}$$

with $d_{0,m} = \sqrt{(x_0 - x_m)^2 + (y_0 - y_m)^2}$.
On the other hand, since the channel from the RIS to the MUs is usually affected by shadowing and blockage, a non-LoS (NLoS) model is applied. In this case then, the channel from the m-th RIS to the (m, k)-th MU is modelled as [30]

$$\begin{aligned}\beta_{m,k} &= PL_{m,k} + \eta^{LoS} P_{m,k}^{LoS} + \eta^{NLoS} P_{m,k}^{NLoS} \\ &= 10\alpha \log\left(\sqrt{d_{m,k}^2 + H_m^2}\right) + AP_{m,k}^{LoS} + B,\end{aligned} \tag{3}$$

where η^{LoS} and η^{NLoS} are the average additional losses for LoS and NLoS, respectively, $A = \eta^{LoS} - \eta^{NLoS}$ and $B = 10\alpha \log(\frac{4\pi l_{m,k}}{\lambda_c}) + \eta^{NLoS}$. The path loss is given as follows:

$$PL_{m,k} = 10 \log(\frac{4\pi l_{m,k}}{\lambda_c})^{\alpha}, \ m = 1, ..., M, \tag{4}$$

where $\lambda_c = c/f_c$ is the wavelength of the carrier at frequency f_c epressed in Hz, while $\alpha \geq 2$ is the path loss exponent. As regards the probability of LoS and NLoS, they are modelled by [31]:

$$P_{m,k}^{LoS} = \frac{1}{1 + a \exp\left[-b\left(\arctan\left(\frac{H_m}{d_{m,k}}\right) - a\right)\right]}, \tag{5}$$

$$P_{m,k}^{NLoS} = 1 - P_{m,k}^{LoS}, \tag{6}$$

whit a and b representing environmental constraints.

Finally, the phase shift matrix at the m-th RIS is expressed as:

$$\mathbf{\Phi}_m = diag[\phi_{1m}, \phi_{2m}, ..., \phi_{Nm}], m \in \mathcal{M} \tag{7}$$

where $diag(\mathbf{a})$ denotes a diagonal matrix having the element of vector $\mathbf{a}$ along its diagonal. More specifically, each coefficient is modelled as $\phi_{nm} = \alpha_{nm} e^{j\theta_{nm}}$ with $\alpha_{nm} \in [0, 1]$ and $\theta_{nm} \in [0, 2\pi]$ $(\forall n = 1, 2, ..., N, \ m \in \mathcal{M})$ indicating the amplitude and phase shift of received by the signal from the n-th reflecting element. It is worth to mention that we assume $\alpha_{nm} = 1$ [32]. In order to take into account the effect of the small scale fading coefficients, we assume that for both BS to m-th RIS, and m-th RIS to the (m, k)-th MU channels, the small-scale fading contributions are modelled as independent and identically distributed random variables with zero mean and unit variance, respectively indicated as $\hat{h}_{0,m} \in \mathbb{C}^{N\times 1}$ and $\hat{h}_{m,k}^H \in \mathbb{C}^{1\times N}$. We also also use $\mathbf{h}_{0,m} \in \mathbb{C}^{N\times 1}$ and $\mathbf{h}_{m,k}^H \in \mathbb{C}^{1\times N}$ to indicate the matrices containing the channel coefficients between the BS and the m-th RIS and the m-th RIS to the (m, k)-th MU in the m-th group, respectively. As result the total channel coefficient from the BS to the (m, k)-th MU through the m-th RIS can be expressed as [33]:

$$\mathbf{g}_{m,k} = \mathbf{h}_{m,k}^H \mathbf{\Phi}_m \mathbf{h}_{0,m}, \ m \in \mathcal{M}, \ k \in \mathcal{K}_m, \tag{8}$$

where $\mathbf{h}_{0,m} = \sqrt{\beta_{0,m}}\hat{h}_{0,m}$ and $\mathbf{h}_{m,k}^H = \sqrt{\beta_{m,k}}\hat{h}_{m,k}^H$.

2.3. Signal Model

As illustrated in Figure 1, we have considered a downlink communication scenario where a signal from a BS is trnasmitted to K single antenna MUs with the support of RISs deployed on buildings facade to help in improving the BS-MUs communication link. Supposing that the communications are performed through the Time Division Multiple Access (TDMA) scheme, the signal at the k-th MU in the m-th group can be expressed as:

$$y_{m,k} = \sqrt{p_{m,k}}\mathbf{g}_{m,k} x_{m,k} + \omega_k, \ m \in \mathcal{M}, \ k \in \mathcal{K}_m, \tag{9}$$

in which $p_{m,k}$ denotes the transmission power allocated by the BS to the (m, k)-th MU, $x_{m,k}$ with $\|x_{m,k}\|^2 \leq 1$ is the informative message, $\omega_k \sim \mathcal{CN}(0, \sigma_k^2)$ is the Additive White Gaussian Noise (AWGN).

indicating with $\boldsymbol{p}_0 = [\boldsymbol{p}_{0,m}]_{m=1}^M$, where $\boldsymbol{p}_{0,m} = [p_{m,k}]_{k=1}^{K_m}$ power control coefficients used at the BS, and with $\mathbf{\Phi}_M = [\mathbf{\Phi}_m]_{m=1}^M$ the phase shifts coefficients of RISs, the SNR at the (m, k)-th MU be formulated as

$$\gamma_{m,k}\left(p_{m,k}, \mathbf{\Phi}_m\right) = \frac{p_{m,k}\left|\mathbf{g}_{m,k}\right|^2}{\sigma_k^2}. \tag{10}$$

Then, the throughput of the (m, k)-th MU, expressed in bit per second per Hertz (bps/Hz) can be expressed using the Shannon formula for the channel capacity:

$$R_{m,k}\left(p_{m,k}, \mathbf{\Phi}_m\right) = \log_2\left(1 + \gamma_{m,k}\left(p_{m,k}, \mathbf{\Phi}_m\right)\right) \tag{11}$$

Finally, the total throughput of all MUs in the considered network can be formulated as

$$R_{total}\left(\boldsymbol{p}_0, \mathbf{\Phi}_M\right) = \sum_{m=1}^{M}\sum_{k=1}^{K_m} R_{m,k}\left(p_{m,k}, \mathbf{\Phi}_m\right). \tag{12}$$

2.4. Problem Formulation

As already mentioned before, we aim at jointly optimizing the power control coefficients $(\boldsymbol{p}_0)$ at the BS and the phase shift $(\mathbf{\Phi}_M)$ of the RISs, in order to maximize the total downlink network throughput, under power consumption and QoS constraints. To this end, we formulated the following optimization problem:

$$\max_{\boldsymbol{p}_0, \mathbf{\Phi}_M} \ R_{total}\left(\boldsymbol{p}_0, \mathbf{\Phi}_M\right) \tag{13a}$$

$$\text{s.t.} \quad \sum_{m=1}^{M}\sum_{k=1}^{K_m} p_{m,k} \leq P_0^{\max}, m \in \mathcal{M}, \ k \in \mathcal{K}_m, \tag{13b}$$

$$R_{m,k}\left(p_{m,k}, \mathbf{\Phi}_m\right) \geq \bar{r}_{m,k}, \ m \in \mathcal{M}, \ k \in \mathcal{K}_m, \tag{13c}$$

$$0 \leq \theta_{nm} \leq 2\pi, \forall n = 1, 2, ..., N, \ m \in \mathcal{M}, \tag{13d}$$

where the constraint (13b) represents the total power consumption constraint at the BS. On the other hand, constraints (13c) and (13d) accounts for the individual QoS requirement at the (m, k)-th MU and lower and upper bounds of the phase shifts of RIS elements, respectively.

3. Proposed Optimization Framework

In order to deal with the non-convexity of problem (13) and its related constraints, we proposed an algorithm that iteratively optimize the power control coefficients at the BS and the phase shifts of RIS reflecting elements. The main components of this algortihm are explained in the following subsections.

3.1. Optimization of Power Control Coefficients

At this stage we assume that $\mathbf{\Phi}_M$ is fixed, then (13) obtaining then the following optimization problem for the power coefficients:

$$\max_{\boldsymbol{p}_0} R_{total}\left(\boldsymbol{p}_0\right) \tag{14a}$$

$$\text{s.t.} \quad (13b), (13c). \tag{14b}$$

This problem is solved by an effective approximation obtained by using logarithm inequalities [34, 35] based on the property that the convex function $f(z) = \log_2(1 + \frac{1}{z}) \geq \hat{f}(z)$, with

$$\hat{f}(z) = \log_2\left(1 + \frac{1}{\bar{z}}\right) + \frac{1}{1+\bar{z}} - \frac{z}{(1+\bar{z})\bar{z}}, \tag{15}$$

$\forall z > 0, \bar{z} > 0$. Then, the throughput expression can be rewritten as:

$$R_{m,k}\left(p_{m,k}\right) \geq \hat{R}_{m,k}^{(iter)}\left(p_{m,k}\right), \ \forall k \in \mathcal{K}_m, \ \forall m \in \mathcal{M}, \tag{16}$$

where

$$z = \frac{\sigma_k^2}{p_{m,k}\left|\boldsymbol{g}_{m,k}\right|^2}, \ \bar{z} = z^{(iter)} = \frac{\sigma_k^2}{p_{m,k}^{(iter)}\left|\boldsymbol{g}_{m,k}\right|^2},$$

$$\hat{R}_{m,k}^{(iter)}\left(p_{m,k}\right) = \log_2\left(1 + \frac{1}{\bar{z}}\right) + \frac{1}{1+\bar{z}} - \frac{z}{(1+\bar{z})\bar{z}}. \tag{17}$$

Then, the optimization problem (14) at the i-th iteration can be rewritten as:

$$\max_{\boldsymbol{p}_0} \hat{R}_{total}^{(iter)}\left(\boldsymbol{p}_0\right) \tag{18a}$$

$$\text{s.t.} \quad (13b), \tag{18b}$$

$$\hat{R}_{m,k}^{(iter)}\left(\boldsymbol{p}_0\right) \geq \bar{r}_{m,k}, \ m \in \mathcal{M}, \ k \in \mathcal{K}_m, \tag{18c}$$

where $\hat{R}_{total}^{(\kappa)}\left(\boldsymbol{p}_0\right) = \sum_{m=1}^{M}\sum_{k=1}^{K_m}\hat{R}_{m,k}^{(\kappa)}\left(p_{m,k}\right)$.
It is noticed that (18) is convex. Thus, it can be solved efficiently by using standard software, such as CVX tools[36]. The proposed iterative power allocation procedure to solve the problem (18) to provide the optimal power control coefficients $(\boldsymbol{p}_0^*)$ is summarized in the Algorithm 1, where the maximum number of iterations is $Iter_{max} = 20$.

Algorithm 1 Power allocation procedure

1: **Initialize**:
2: Let the iteration value $iter = 0$ and $Iter_{max} = 20$
3: Let the feasible point for $\mathbf{\Phi}_M$, and the tolerance $\xi = 10^{-3}$
4: **while** (The convergence is not reach or $iter \leqslant I_{max}$)
5: Solve (18) to find $(\boldsymbol{p}_0^{(i+1)})$ using CVX tool
6: Update $iter = iter + 1$
7: **end while**
8: **Output**: the optimal power control coefficients $\boldsymbol{p}_0^*$

3.2. Phase Shift Optimization

Similarly, we assume that power control coefficients $\boldsymbol{p}_0$ is fixed, thus the problem (13) can be rewritten as follows:

$$\max_{\mathbf{\Phi}_M} R_{total}\left(\mathbf{\Phi}_M\right) \tag{19a}$$

$$\text{s.t.} \quad (13c), (13d). \tag{19b}$$

In this problem we introduce the notation for the cascaded channel $\boldsymbol{h}_{m,k}^H\mathbf{\Phi}_m\boldsymbol{h}_{0,m} = \upsilon_m^H\chi_{m,k}$ where $\upsilon_m = [\upsilon_m^1, ..., \upsilon_m^N]^H$ with $\upsilon_m^n = e^{j\theta_{nm}}$ $(\forall n = 1, 2, ..., N)$, $\chi_{m,k} = diag(\boldsymbol{h}_{m,k}^H)\boldsymbol{h}_{0,m}$, and $\rho_k = P_0/\sigma_k^2$. Supposing $|\upsilon_m^n|^2 = 1$, the (13d) constraints becomes the unit-modulus constraint [37]. Then, the problem (19) is equivalent to the following:

$$\max_{\upsilon_m, \ m\in\mathcal{M}} \sum_{m=1}^{M}\sum_{k=1}^{K_m}\log_2\left(1 + \rho_k\upsilon_m^H\chi_{m,k}\chi_{m,k}^H\upsilon_m\right) \tag{20a}$$

$$\text{s.t.} \quad \upsilon_m^H\chi_{m,k}\chi_{m,k}^H\upsilon_m \geq \left(2^{\bar{r}_{m,k}} - 1\right)/\rho_k, \tag{20b}$$

$$|\upsilon_m^n|^2 = 1, \forall n = 1, 2, ..., N, \ m \in \mathcal{M}. \tag{20c}$$

Since (20) is still non-convex we used a relaxation method in order to obtain a convex version of this optimization problem. In particular, we first denote $\mathbf{X}_{m,k} = \chi_{m,k}\chi_{m,k}^H$ and $\upsilon_m^H\mathbf{X}_{m,k}\upsilon_m = tr\left(\mathbf{X}_{m,k}\upsilon_m\upsilon_m^H\right) = tr\left(\mathbf{X}_{m,k}\mathbf{\Upsilon}_m\right)$ where $\mathbf{\Upsilon}_m = \upsilon_m\upsilon_m^H$ satisfies the condition $\mathbf{\Upsilon}_m \succeq \mathbf{0}$ and rank($\mathbf{\Upsilon}_m$)=1, $\forall m \in \mathcal{M}$. This allowed us to relax the rank-one constraint of (20c) [38]. Finally, (20) can be rewritten as:

$$\max_{\upsilon_m, \ m\in\mathcal{M}} \sum_{m=1}^{M}\sum_{k=1}^{K_m}\log_2\left(1 + \rho_k tr\left(\mathbf{X}_{m,k}\mathbf{\Upsilon}_m\right)\right) \tag{21a}$$

$$\text{s.t.} \quad tr\left(\mathbf{X}_{m,k}\mathbf{\Upsilon}_m\right) \geq \left(2^{\bar{r}_{m,k}} - 1\right)/\rho_k, \tag{21b}$$

$$\mathbf{\Upsilon}_{m(n,n)} = 1, \forall n = 1, 2, ..., N, \ m \in \mathcal{M}, \tag{21c}$$

$$\mathbf{\Upsilon}_m \succeq \mathbf{0}. \tag{21d}$$

Problem (21) is a convex semidefinite program (SDP) [37], which can be efficiently solved by using

CVX tool. Algorithm 2 illustrate the proposed Block Coordinate Descendent (BCD) method employed to find the optimal phase shift ($\mathbf{\Phi}_M^*$).

Algorithm 2 Phase shift searching procedure

1: **Initialize**:
2: Let the iteration value $iter = 0$ and $Iter_{max} = 20$
3: Let the feasible point for $\boldsymbol{p}_0$, $\xi = 10^{-3}$, and $\boldsymbol{f}_{m,k}^{(0)}$
4: **while** (The convergence is not reach or $iter \leqslant I_{max}$)
5: **for** m in range $[1 : M]$
6: Solve (21) to find ($\mathbf{\Phi}_M^{(iter+1)}$) using CVX tool
7: Update $\boldsymbol{f}_{m,k}^{(iter+1)}$
8: **end for**
9: Update $iter = iter + 1$
10: **end while**
11: **Output**: The optimal phase shift $\mathbf{\Phi}_M^*$

Then, the intractable optimization problem in (13) is solved by combining the Algorithm 1 power allocation optimization and Algorithm 2 RIS phase shift optimization.

4. Simulation Results

Table 2. Simulation Parameters

Parameter	Value
Radius of BS's coverage circle	500m
Radius of expanded deployment	1500m
BS's location	(0,0,30)m
White noise power density	-130 dBm/Hz
QoS threshold	1 bps/Hz
Tolerance for convergence of algorithm	$\xi = 10^{-3}$
Bandwidth	10MHz
BS transmit power	[43:46]dBm
Number of users in small cell	[20, 30]
Number of RISs	[4, 8, 12, 20]
Number of reflecting elements	[100, 150, 200, 250, 300]

In this section, we illustrate the performances of our proposed optimization method obtained through numerical simulation carried out using Matlab. To perform the simulation, we use the personal computer with CPU Intel(R) Core(TM) i7-9700 CPU @ 3.00GHz and 16GB memory. Simulation parameters are summarized in Table 2. As regards the channel modelling we considered the same settings adopted in [34, 39]. The performances of our proposed method, indicated as **(OOP)**, have been compared with the performances achieved by oter conventional methods such as Optimal power allocation with Random phase shift **(ORP)** , and Equal power allocation with Optimal phase shift

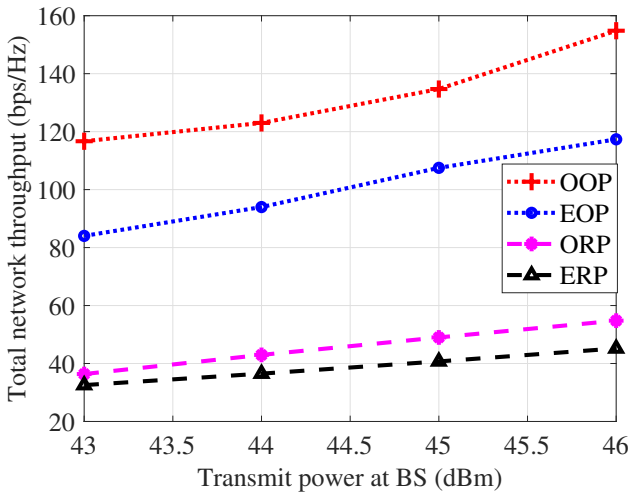

Figure 2. Total network throughput versus transmission power at BS with $M = 4$, $K = 20$, $N = 200$.

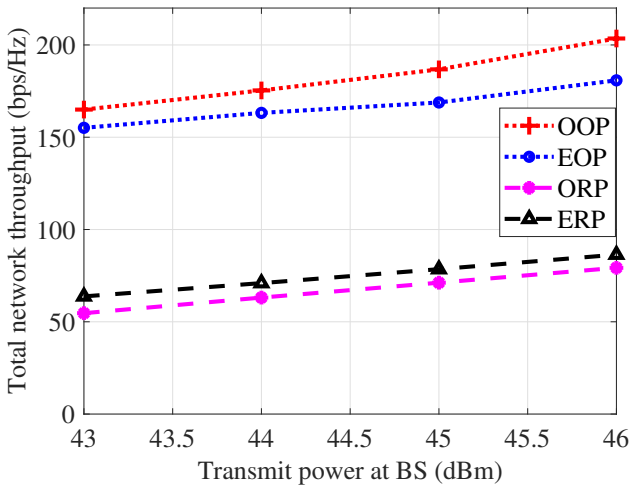

Figure 3. Total throughput versus transmission power at BS with $M = 8$, $K = 30$, $N = 200$.

(EOP) demonstrate the results in case of either without optimizing power allocation or without phase shift optimization, respectively. Additional, the Equal power allocation - Random phase shift **(ERP)** has also been considered, which is the one not optimizing neither power allocation nor phase shift coefficients.

4.1. The total network throughput

To demonstrate the outperform of jointly optimization problem, we show the results in difference scenarios obtained by changing maximum transmit power, number of RIS, and number of reflecting elements per RIS. To take into account the effect of both number of RIS and number of MU in each group of user, Figure 2 illustrates how the total network throughput

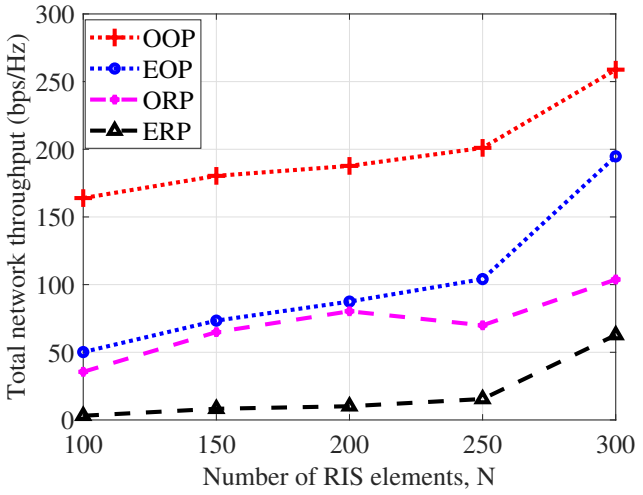

Figure 4. Total throughput versus number of reflecting elements ($M = 8$, $K = 30$, $P_0^{\max} = 46$ dBm).

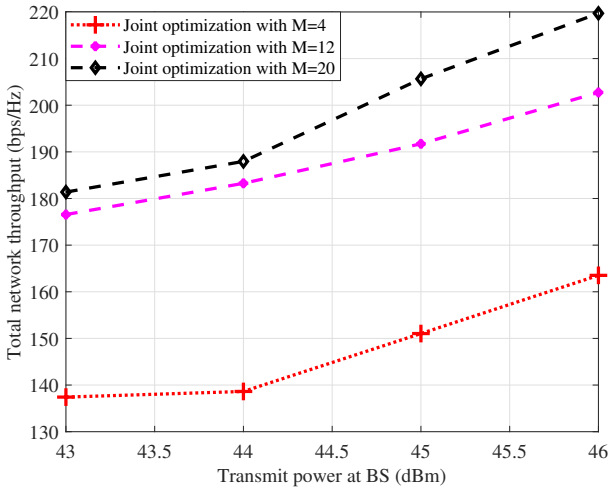

Figure 5. Total network throughput of the proposed method jointly optimization with different number of RISs ($M = 4$, $M = 12$, $M = 20$).

varies when he number of RISs and the number of UEs are $M = 4$ and $K = 20$, respectively. Similarly, Figure 3 illustrates the case when $M = 8$ and $K = 30$. In both cases, the number of reflecting elements per RIS is fixed to $N = 200$. As a general trend, one can easily note how the total network throughput increases as the transmit power at the BS increases too. In addition, from these two figures we can also observe how the gap between the proposed method (**OOP**) and the **ERP** becomes bigger as the transmit power goes up. Last but not least, the total network throughput also increases number of RISs in the scenario. We can then state that the consider method, where the optimal phase shift is obtained through Algorithm 2, result to be more efficient than the others in all scenarios in Figure 2 and Figure 3. It is obvious the **OOP** achieved approximately four times higher than the **ERP** without optimization at $P_0^{\max} = 45$ dBm with $M = 30$, $K = 30$, and $N = 200$ in Figure 3.

We also illustrate how the total network throughput varies with different number of reflecting elements per RIS, which in Figure 4 vary from 100 to 300 while $M = 8$, $K = 30$, and $P_0^{\max} = 46$ dBm. In this case, it can also be observed how to an increase of number of reflecting elements corresponds an increase of the total network throughput. In particular, as exptected, it can be noted how the total network throughput achieved though the **OOP** is significantly larger than others resource allocation schemes. Particularly, it can achieve approximately a four times higher throughput when compared with the **ERP**. Finally, the results in Figure 5 demonstrate the total network throughput of obtained by the proposed method by varying the number of RIS, i.e., $M = 4$, $M = 12$, and $M = 20$, respectively. Also in this case, it can be observed how the total network

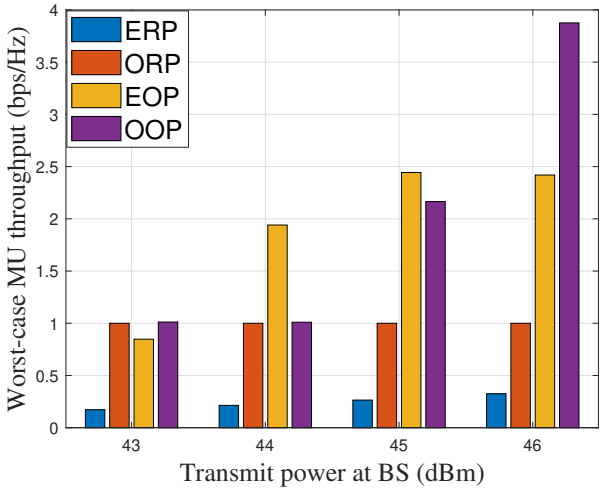

Figure 6. Worst-case MU throughput versus transmit power at BS ($M = 8$, $K = 30$, $N = 200$).

throughput increases significantly when the number of RIS rises from $M = 4$ to $M = 20$. Particularly, the gap of throughput between $M = 4$ to $M = 20$ changes steeply when the transmit power increase from $44dBm$ to $46dBm$, i.e., approximately $56bps/Hz$ at peak transmit power $46dBm$.

4.2. The worst-case MU throughput

In this part, we consider the total network throughput of the worst-case MU in order to prove the proposed method outperform when compared with conventional scheme also in this case.

As expected, the result in Figure 6 demonstrates the superiority of the proposed method (**OOP**) compared

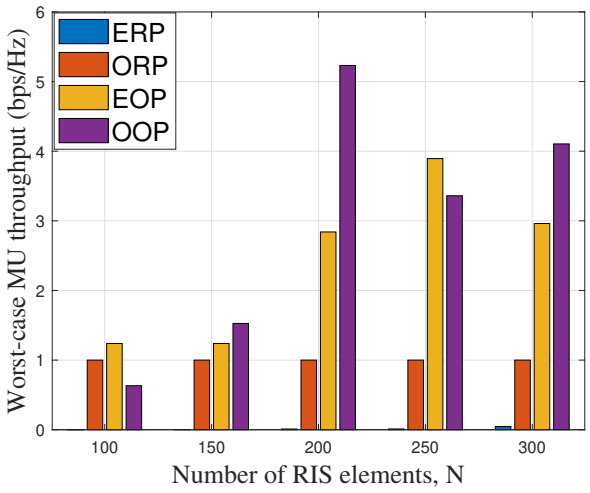

Figure 7. Worst-case MU throughput versus number of RIS elements N ($M = 20$, $K = 30$, $P_0^{\max} = 46dBm$).

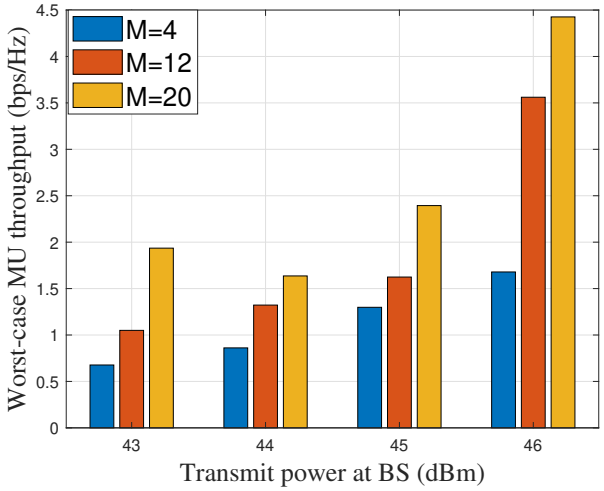

Figure 8. Worst-case MU throughput of the proposed method jointly optimization with different number of RISs ($M = 4$, $M = 12$, $M = 20$).

to the conventional schemes including **OPH**, **EOP**, and **ERP**, respectively, in case of worst-case MU throughput when the values are fixed at $M = 8$, $K = 30$, and $N = 200$. At the onset, it is clear that the worst MU throughput of **OOP** is equal to 1 bps/Hz at $P_0^{\max} = 43dBm$, and $P_0^{\max} = 44dBm$, while at $P_0^{\max} = 45dBm$, and $P_0^{\max} = 46dBm$ are higher and reach the peak value approximately double at $P_0^{\max} = 46dBm$. Likewise, **ORP** achieves a 1 bps/Hz thoguhput when the transmit power of BS grows up from $P_0^{\max} = 43dBm$ to $P_0^{\max} = 46dBm$, meanwhile the worst MU throughput of **EOP** increase when the transmit power increases. However, without optimization **ERP**, the worst MU throughput is less than 0.5 bps/Hz, so it is unsatisfied the individual QoS constraints in (13c).

On the other hand, to prove the effect of the number of reflecting element per RIS, in Figure 7, we plot the worst-case MU throughput by fixing $P_0^{\max} = 46dBm$), $M = 20$, $K = 30$, while the number of reflecting elements ranges from 100 to 300. In this case , it can be noticed that the throughput achieved by the worst-cse MU mostly satysfies the individual QoS constraint expressed in (13c) with the value higher than $1bps/Hz$, except when the minimum considered transmit power $P_0^{\max} = 43dBm$ is considered. Conversely, it is obvious the when no optimization is applied, i.e., **ERP**, the MU throughput of the worst-case MU is nearly equal to zero even if the number of reflecting element increases. On the other hand, Figure 8 shows the worst-case MU throughput achieved by varying the number of RIS ($M = 4$, $M = 12$, $M = 20$), while the number of reflecting element is fixed to $N = 200$, and the number of user in each small cell is fixed to $K = 30$. It can be seen from this figure that in the majority of cases the MU throughput of the proposed method is mostly greater than 1 bps/Hz, as well as how the perceived throughput increases when the number of RISs and the transmit power of BS increase too. Last but not least, the MU throughput at $M = 20$ is approximately 2.5 times higher than MU throughput at $M = 12$ when the transmit power is set at $P_0^{\max} = 43dBm$.

5. Conclusions and Future Directions

In this paper, we have investigated how the integration of RIS can improve the network performances of SISO downlink cellular wireless networks. Specifically, our focus has been on optimizing the total network throughput under the constraints of maximum transmit power at the BS and QoS requirements of users. To address this challenge, we formulated a related optimization problem, for which we have introduced an iterative algorithm that jointly optimizes the power allocation and phase shift of RISs. The numerical results outlined the efficacy of our proposed system when compared to other conventional resource allocation schemes. In particular it has been illustrated how the total network throughput can be highly maximized when both power allocation and phase shift are optimized. Furthermore, even in worst-case MU scenarios throughput, the proposed methods demonstrates superior performance when power allocation and phase shift coefficients are jointly optimized. As future research direction, we will extend this work by considering multiple antennas BS, and then introducing the active beamforming at BS into the optimization problem.

Acknowledgements

This paper is supported by Ho Chi Minh City University of Technology and Education, Vietnam.

References

[1] Truong PQ, Van CP. Reconfigurable Intelligent Surfaces for Downlink Cellular Networks. In: Vo NS, Vien QT, Ha DB, editors. Industrial Networks and Intelligent Systems. Cham: Springer International Publishing; 2022. p. 20-32.

[2] ITU-R. IMT Traffic Estimates for the Years 2020 to 2030; 2015.

[3] Bui TT, Nguyen LD, Kha HH, Vo NS, Duong TQ. Joint Clustering and Resource Allocation Optimization in Ultra-Dense Networks with Multiple Drones as Small Cells Using Game Theory. Sensors. 2023;23(8). Available from: https://www.mdpi.com/1424-8220/23/8/3899.

[4] Wikström G, Peisa J, Rugeland P, Johansson N, Parkvall S, Girnyk M, et al. Challenges and Technologies for 6G. In: 2020 2nd 6G Wireless Summit (6G SUMMIT); 2020. p. 1-5.

[5] Wang CX, Huang J, Wang H, Gao X, You X, Hao Y. 6G Wireless Channel Measurements and Models: Trends and Challenges. IEEE Vehicular Technology Magazine. 2020;15(4):22-32.

[6] Gong S, Lu X, Hoang DT, Niyato D, Shu L, Kim DI, et al. Toward Smart Wireless Communications via Intelligent Reflecting Surfaces: A Contemporary Survey. IEEE Communications Surveys Tutorials. 2020;22(4):2283-314.

[7] Nguyen KK, Masaracchia A, Yin C. Deep Reinforcement Learning for Intelligent Reflecting Surface-assisted D2D Communications. EAI Endorsed Transactions on Industrial Networks and Intelligent Systems. 2023 Jan;10(1):e1. Available from: https://publications.eai.eu/index.php/inis/article/view/2864.

[8] Strinati EC, Alexandropoulos GC, Wymeersch H, Denis B, Sciancalepore V, D'Errico R, et al. Reconfigurable, Intelligent, and Sustainable Wireless Environments for 6G Smart Connectivity. IEEE Commun Mag. 2021 Oct;59(10):99-105.

[9] Alghamdi R, Alhadrami R, Alhothali D, Almorad H, Faisal A, Helal S, et al. Intelligent Surfaces for 6G Wireless Networks: A Survey of Optimization and Performance Analysis Techniques. IEEE Access. 2020;8:202795-818.

[10] Boulogeorgos AAA, Alexiou A. Performance Analysis of Reconfigurable Intelligent Surface-Assisted Wireless Systems and Comparison With Relaying. IEEE Access. 2020;8:94463-83.

[11] Tao Q, Wang J, Zhong C. Performance Analysis of Intelligent Reflecting Surface Aided Communication Systems. IEEE Communications Letters. 2020;24(11):2464-8.

[12] Kudathanthirige D, Gunasinghe D, Amarasuriya G. Performance Analysis of Intelligent Reflective Surfaces for Wireless Communication. In: ICC 2020 - 2020 IEEE International Conference on Communications (ICC); 2020. p. 1-6.

[13] Cheng Y, Li KH, Liu Y, Teh KC. Outage Performance of Downlink IRS-Assisted NOMA Systems. In: GLOBECOM 2020 - 2020 IEEE Global Communications Conference; 2020. p. 1-6.

[14] Huang C, Zappone A, Alexandropoulos GC, Debbah M, Yuen C. Reconfigurable Intelligent Surfaces for Energy Efficiency in Wireless Communication. IEEE Transactions on Wireless Communications. 2019;18(8):4157-70.

[15] Guo H, Liang YC, Chen J, Larsson EG. Weighted Sum-Rate Maximization for Reconfigurable Intelligent Surface Aided Wireless Networks. IEEE Transactions on Wireless Communications. 2020;19(5):3064-76.

[16] Cao Y, Lv T, Ni W. Intelligent Reflecting Surface Aided Multi-User mmWave Communications for Coverage Enhancement. In: 2020 IEEE 31st Annual International Symposium on Personal, Indoor and Mobile Radio Communications; 2020. p. 1-6.

[17] Perović NS, Tran LN, Di Renzo M, Flanagan MF. Achievable Rate Optimization for MIMO Systems With Reconfigurable Intelligent Surfaces. IEEE Transactions on Wireless Communications. 2021;20(6):3865-82.

[18] Li Y, Yin C, Do-Duy T, Masaracchia A, Duong TQ. Aerial Reconfigurable Intelligent Surface-Enabled URLLC UAV Systems. IEEE Access. 2021;9:140248-57.

[19] Masaracchia A, Li Y, Nguyen KK, Yin C, Khosravirad SR, Costa DBD, et al. UAV-Enabled Ultra-Reliable Low-Latency Communications for 6G: A Comprehensive Survey. IEEE Access. 2021;9:137338-52.

[20] Nguyen KK, Masaracchia A, Sharma V, Poor HV, Duong TQ. RIS-Assisted UAV Communications for IoT With Wireless Power Transfer Using Deep Reinforcement Learning. IEEE J Sel Topics Signal Process. 2022;16(5):1086-96.

[21] Li S, Duo B, Yuan X, Liang YC, Di Renzo M. Reconfigurable Intelligent Surface Assisted UAV Communication: Joint Trajectory Design and Passive Beamforming. IEEE Wireless Communications Letters. 2020;9(5):716-20.

[22] Nguyen KK, Khosravirad SR, da Costa DB, Nguyen LD, Duong TQ. Reconfigurable Intelligent Surface-Assisted Multi-UAV Networks: Efficient Resource Allocation With Deep Reinforcement Learning. IEEE Journal of Selected Topics in Signal Processing. 2022;16(3):358-68.

[23] Ren H, Zhang Z, Peng Z, Li L, Pan C. Energy Minimization in RIS-Assisted UAV-Enabled Wireless Power Transfer Systems. IEEE Internet of Things Journal. 2023;10(7):5794-809.

[24] Nguyen MHT, Garcia-Palacios E, Do-Duy T, Dobre OA, Duong TQ. UAV-Aided Aerial Reconfigurable Intelligent Surface Communications With Massive MIMO System. IEEE Transactions on Cognitive Communications and Networking. 2022;8(4):1828-38.

[25] Ha DB, Truong VT, Lee Y. Intelligent Reflecting Surface assisted RF Energy Harvesting Mobile Edge Computing NOMA Networks: Performance Analysis and Optimization. EAI Endorsed Transactions on Industrial Networks and Intelligent Systems. 2022 Aug;9(32):e5. Available from: https://publications.eai.eu/index.php/inis/article/view/1376.

[26] Merluzzi M, Costanzo F, Katsanos KD, Alexandropoulos GC, Di Lorenzo P. Power Minimizing MEC Offloading

with QoS Constraints over RIS-Empowered Communications. In: GLOBECOM 2022 - 2022 IEEE Global Communications Conference; 2022. p. 5457-62.
[27] Xu Y, Zhang T, Liu Y, Yang D, Xiao L, Tao M. Computation Capacity Enhancement by Joint UAV and RIS Design in IoT. IEEE Internet of Things Journal. 2022;9(20):20590-603.
[28] Nguyen MN, Nguyen LD, Duong TQ, Tuan HD. Real-Time Optimal Resource Allocation for Embedded UAV Communication Systems. IEEE Wireless Communications Letters. 2019;8(1):225-8.
[29] Bor-Yaliniz RI, El-Keyi A, Yanikomeroglu H. Efficient 3-D placement of an aerial base station in next generation cellular networks. In: IEEE ICC; 2016. p. 1-5.
[30] Mozaffari M, Saad W, Bennis M, Debbah M. Efficient Deployment of Multiple Unmanned Aerial Vehicles for Optimal Wireless Coverage. IEEE Commun Lett. 2016 Aug;20:1647-50.
[31] Al-Hourani A, Kandeepan S, Lardner S. Optimal LAP Altitude for Maximum Coverage. IEEE Wireless Communications Letters. 2014;3(6):569-72.
[32] Xie X, Fang F, Ding Z. Joint Optimization of Beamforming, Phase-Shifting and Power Allocation in a Multi-cluster IRS-NOMA Network. IEEE Trans Veh Technol. 2021:1-1.
[33] Wu Q, Zhang R. Beamforming Optimization for Wireless Network Aided by Intelligent Reflecting Surface With Discrete Phase Shifts. IEEE Trans Commun. 2020;68(3):1838-51.
[34] Nguyen LD, Tuan HD, Duong TQ, Dobre OA, Poor HV. Downlink Beamforming for Energy-Efficient Heterogeneous Networks With Massive MIMO and Small Cells. IEEE Transactions on Wireless Communications. 2018;17(5):3386-400.
[35] Duong T. Real Time Convex Optimisation for 5G Networks and Beyond. Institution of Engineering and Technology (IET); 2021.
[36] Grant M, Boyd S. CVX: MATLAB Software for Disciplined Convex Programming, version 2.1; 2014. http://cvxr.com/cvx.
[37] Wu Q, Zhang R. Intelligent Reflecting Surface Enhanced Wireless Network via Joint Active and Passive Beamforming. IEEE Trans Wireless Commun. 2019;18(11):5394-409.
[38] Yu H, Tuan HD, Nasir AA, Duong TQ, Poor HV. Joint Design of Reconfigurable Intelligent Surfaces and Transmit Beamforming Under Proper and Improper Gaussian Signaling. IEEE Journal on Selected Areas in Communications. 2020;38(11):2589-603.
[39] Do-Duy T, Nguyen LD, Duong TQ, Khosravirad S, Claussen H. Joint Optimisation of Real-time Deployment and Resource Allocation for UAV-Aided Disaster Emergency Communications. IEEE Journal on Selected Areas in Communications. 2021:1-1.

IEEE Access
Multidisciplinary | Rapid Review | Open Access Journal

Received 10 July 2024, accepted 25 July 2024, date of publication 29 July 2024, date of current version 14 August 2024.

Digital Object Identifier 10.1109/ACCESS.2024.3435483

RESEARCH ARTICLE

Computation Offloading and Resource Allocation Optimization for Mobile Edge Computing-Aided UAV-RIS Communications

PHUC Q. TRUONG[1], TAN DO-DUY[1], (Member, IEEE), ANTONINO MASARACCHIA[2,3], (Senior Member, IEEE), NGUYEN-SON VO[4,5], (Senior Member, IEEE), VAN-CA PHAN[1], DAC-BINH HA[4,5], AND TRUNG Q. DUONG[2,6], (Fellow, IEEE)

[1]Department of Computer and Communication Engineering, Faculty of Electrical and Electronics Engineering, Ho Chi Minh City University of Technology and Education, Ho Chi Minh City 700000, Vietnam
[2]School of Electronics, Electrical Engineering and Computer Science, Queen's University Belfast, BT7 1NN Belfast, U.K.
[3]School of Electronic Engineering and Computer Science, Queen Mary University of London, E1 4NS London, U.K.
[4]Institute of Fundamental and Applied Sciences, Duy Tan University, Ho Chi Minh City 700000, Vietnam
[5]Faculty of Electrical-Electronic Engineering, Duy Tan University, Da Nang 550000, Vietnam
[6]Faculty of Engineering and Applied Science, Memorial University of Newfoundland, St. John's, NL A1C 5S7, Canada

Corresponding author: Dac-Binh Ha (hadacbinh@duytan.edu.vn)

This work was supported by Vietnam National Foundation for Science and Technology Development (NAFOSTED) under Grant 102.04-2021.11.

ABSTRACT The concept of Mobile Edge Computing (MEC) has been recently highlighted as a key enabling technology for the deployment of sixth-generation (6G) wireless network services. On the other hand, the possibility of combining Unmanned Aerial Vehicles (UAV) with Reconfigurable Intelligent Surfaces (RIS) has also been recognized as a powerful communication paradigm able to provide improved propagation characteristics of wireless communication channels, as well as increased capacity and extended coverage. Then, the possibility of merging the characteristics of such a communication paradigm with the one provided through MEC represents a valid solution to fulfill the main requirements of 6G networks. In this paper, we consider the combination of computation offloading and resource allocation in an MEC-based system where the MEC server is hosted by a massive MIMO base station, which serves multiple macro-cells assisted by a UAV-equipped RIS. In this context, we focus on minimising the latency for executing tasks of all user equipment (UE) within the considered scenario. To tackle this problem, we formulate an optimisation problem that jointly optimises computation offloading from user equipment (UE) towards the MEC server, and communication resources in the underlying UAV-assisted and RIS-aided network. The extensive simulation results demonstrate how the proposed method outperforms in terms of providing reduced latency for the considered system when compared with other conventional schemes.

INDEX TERMS Computation offloading, mobile edge computing, reconfigurable intelligent surfaces, resource allocation, unmanned aerial vehicle.

I. INTRODUCTION

Wthin the last two decades, wireless communication technologies have undergone a rapid advancement process, leading to the development of smaller, more portable, and intelligent mobile devices. This process has marked the dawn of the Internet of Things (IoT) era. On the one hand, the widespread use of such devices has paved and still continues to pave the way for the deployment of innovative services, which constantly simplify and enhance our daily lives. However, according to the International Telecommunication Union (ITU), such exponential diffusion of portable devices is expected to lead to a significant rise in global mobile subscribers, projected to reach approximately 17 billion by 2030, with a corresponding generation of data traffic envisaged to soar to around 5 zettabytes per month [1].

The associate editor coordinating the review of this manuscript and approving it for publication was Yeon-Ho Chung.

This represents clear evidence that shortly we may assist to a collapse of the fifth-generation (5G) network technology if adequate actions are not taken. Indeed, such collapse will be mainly caused by the deployment of new capacity-hungry communication use cases and services such as multi-sensory extended reality, autonomous vehicles, industrial automation, healthcare systems, and video streaming, which are envisioned to be delivered within the upcoming years. [2]. However, the evolution of wireless networks must extend beyond the possibility to create more capacity to accommodate this surge. Indeed, next-generation networks must also deliver real-time communication with near-zero latency (communication lags less than 1 ms) and ultra-reliable transmission, i.e., less than 10^{-5} of communication error probability. These features are expected to become a reality through the full roll-out of 6G mobile communication systems [3], [4].

Furthermore, 6G technology is also expected to provide improved communication efficiency and intelligent data processing features for smart connected devices [5]. Within this regard, one approach that has gained particular attention within the last few years is the so-called MEC paradigm. With such an approach, computationally intensive tasks can be either partly or entirely offloaded and executed at the MEC servers, which are usually put at the edge of networks [6], [7], [8]. In this way, IoT devices with limited computational capabilities can offload the execution of the task to the edge server, reducing then the latency of the application, as well as increasing their operational lifetime since they are also energy-constrained. Then, one can easily notice why MEC has been highlighted as a valid candidate to provide improvements to next-generation wireless networks in terms of reduced latency and improved energy efficiency [8].

Nevertheless, the full deployment of 6G networks is also strongly dependent on providing innovative technologies that can improve the propagation characteristics of the wireless channel. Indeed, 6G communication scenarios will be highly complex and subject to strong high penetration losses of communication signals since THz communications are expected to be supported. This problem has been partly addressed with the introduction of massive multiple-input multiple-output (mMIMO) and hybrid analog and digital beamforming technologies [9], [10]. However, designing highly efficient multi-antenna transceivers for beamforming on THz bandwidth is challenging. To this end two main solutions have been identified as valid candidates to provide improvements at the physical layer: *i)* UAV-based communications, and *ii)* RIS-assited communication environments. Indeed, the main distinctive feature of UAV-based communications, when compared to conventional static base station (BS) communication, is the possibility of establishing line-of-sight (LoS) communication between UAV, acting as flying BS, and ground users. In this way, it will be possible to offer increased signal strength, which in turn enables the possibility to increase network performances [11]. On the other hand, RIS are entirely programmable metasurfaces, typically placed on a building facade, that through the usage of appropriate external signals allow to reflect the wireless signal in the desired direction. In this way, RIS can be employed to provide additional sources of links with the main aim of compensating for path loss and channel sparsity, enhancing then the effective connections between the base station and users [12]. Interestingly, the possibility of merging the benefits of these two physical layer solutions by realizing RIS-assisted UAV communications is also receiving a lot of attention [13], [14], [15].

Then, from the above discussions, one can easily observe how the possibility of implementing MEC-based solutions over underlying RIS-assisted UAV communications holds great potential for the deployment of the next generation of wireless networks. Some of the most relevant work presented in the literature on these novel research areas are discussed in the next section.

A. RELATED WORKS

As previously mentioned, the idea of integrating the advantages of LoS transmissions, through the adoption of UAVs, with the potential of implementing RIS to create a smart and controllable propagation environment is gaining attention as a compelling future research direction contributing to the deployment of next-generation wireless networks.

For example, authors in [13] considered a communication scenario where multiple UAVs equipped with an onboard RIS are used to support transmission subject to Ultra-reliable and low-latency communication (URLLC) constraints. In this case, each UAV acts as a repeater aimed at reflecting the signal from a macro BS to all users in the networks located in different areas far away from the BS. For such a communication scenario, authors formulated an optimisation problem for jointly optimising UAVs' deployment, power allocation at BS, phase-shift of RIS, and blocklength of URLLC transmission blocks. Such complex and non-convex optimisation problem, aimed at maximizing communication reliability and fairness among users, has been solved by adopting a deep neural network (DNN) based solution. Through numerical it has been highlighted the great potentialities of aerial RIS in supporting stringent URLLC demands.

Another work focused on showing the potentialities of aerial RIS in further extending the coverage range of massive multiple-input multiple-output (mMIMO) networks has been presented in [16]. In this case, the authors considered an optimisation problem to maximize the total network throughput by finding the optimal power control coefficients at the BS and the phase shift coefficients of the multiple RISs used in the system. By solving this optimisation problem through an iterative algorithm, authors illustrated how aerial RISs can achieve higher levels of network throughput as well as improvement for the users with worst-case throughput and less computational complexity when compared with other benchmark schemes.

On the other hand, the investigation on how UAV-enabled communications can contribute to further improving the performance of MEC systems represents another important research direction. Under this perspective, the optimal computation and communication resource allocation problem for UAV-assisted MEC systems under a non-orthogonal multiple access (NOMA) scheme has been considered in [17]. More specifically, they considered a communication scenario where a UAV serves as a MEC server-equipped flying base station (UAV-MEC). Under these assumptions, an iterative algorithm for jointly optimising user association, transmit power, and computing capacity allocation in order to minimise the total latency of UEs was proposed. Through numerical simulations, it has been highlighted how the proposed scheme outperforms other benchmark schemes in terms of offering overall reduced communication latency for the underlying UEs. Noteworthy, the usage of underlying NOMA communications resulted to provide better performances when compared with conventional orthogonal frequency-division multiple access (OFDMA) systems.

The possibility of reducing task offloading latency in MEC-based systems through the adoption of RIS has been studied in [18]. In this case, they considered a RIS-aided wireless MEC system for heterogeneous networks (HetNet). For such a setting, they formulated the optimisation problem for minimizing the overall system delay by jointly optimising caching, task offloading, and computing resources for the MEC system, as well as resource allocation for the RIS and BS sides. To deal with the resulting NP-hard mixed integer nonlinear programming problem, they proposed a two-stage optimisation algorithm. Through numerical results, it has been shown how the adoption of RIS represents a very effective solution to greatly reduce the task computing delay in MEC HetNet systems.

Recently, possibilities of fully integrating RIS and UAV technologies into MEC-based systems have been also investigated. A novel RIS-enhanced and UAV-assisted MEC framework with underlying NOMA communication has been investigated in [19]. More specifically, in this case, authors supposed that a single-antenna UAV is employed to offload the computation tasks to single antenna ground access points (APs) with the assistance of a RIS. To maximise the UAV's computation capacity, they proposed a two steps optimisation algorithm that jointly optimise the reflecting phase shift of the RIS, communication, and computation (2C) resource allocation, decoding order, and UAV's deployment which was supposed to be static. The numerical results provided within this study demonstrated that the computation capacity is greatly improved with such an approach when compared with other solutions proposed in the literature. A similar work has been presented in [20]. In this case, it has been supposed that the UAV acts as a relay node for supporting multiple offloading computation tasks to remote access points from ground users, through the assistance of the RIS. Also in this case the usage of NOMA as a communication paradigm was considered. However, in this case, authors considered the possibility for the UAV to dynamically moving within an optimal trajectory. Under these assumptions, a method for jointly optimising computation and offloading bits, RIS phase shift design, bandwidth allocation, and the trajectory of the UAV was proposed. Through this study, authors illustrated how the considered system can provide enhanced computation capacity, as well as how the inclusion of RIS and NOMA impact finding the optimal trajectory for the UAV.

B. MOTIVATION AND CONTRIBUTIONS

Based on the previous discussion, is evident how the possibility of implementing MEC systems assisted by the usage of both UAV and RIS technologies is gaining a lot of attention by the research community. More specifically, it has been highlighted how the complete integration of both technologies [19], [20] can provide higher benefits when compared with the exclusive inclusion of a single technology, i.e., UAV-based MEC systems [13], [16] or RIS-assisted MEC systems [18]. However, to the best of the author's knowledge, the majority of works focused on building such unified network, i.e., including both UAV and RIS, have considered RIS installed on the facade of buildings.

Under these perspectives, in this paper, we considered the optimisation problem of computation offloading and resource allocation for MEC systems assisted by a RIS-equipped UAV. A similar work in terms of communication environment has been presented in [21], in which authors aimed at maximising the energy efficiency of a single-antenna communication system. In contrast, this paper provides the following contributions to the current state of the art:

- We propose a novel optimisation framework for a MEC system, hosted within a massive MIMO Base Station (MBS), assisted by the usage of a RIS-equipped UAV able to fly within the coverage area. For such a system, we formulated an optimisation problem aimed at minimising the system latency by jointly optimising the power allocation of each user, user association, phase shift configuration of RIS reflecting elements, and computing resource allocation at the MBS subject to the MBS's computing resource constraints and QoS requirements.
- We design an iterative algorithm to efficiently solve the proposed optimisation problem by applying some approximation and inequalities, path following, and block coordinate descent (BCD) methods. An algorithm for determining the UAV trajectory based on the density of ground users is also provided.
- By means of extensive simulation results, we show that our proposed method outperforms the benchmark strategies indicating the effectiveness of our proposed method.

The remainder of this paper is organized as follows. The considered system model is presented in Section II. Section III provides the formulation of the optimisation problem for latency reduction, as well as the proposed methodology.

The effectiveness of the proposed algorithm in minimising the total system latency is illustrated in Section IV. Finally, conclusions and future research directions are provided in Section V.

II. MEC SYSTEM MODEL

A. SYSTEM MODEL

As illustrated in Figure 1, we consider a mMIMO communication system, which provides coverage extension between the MBS and distributed users (UEs) (e.g., mobile users, vehicles, internet-of-thing (IoT) sensors) through the assistance of assisted a RIS-equipped UAV. In this case, the support of RIS, combined with the flexible deployment of UAV, allows to provide enhanced network performances, in terms of reliable wireless network operation with high quality-of-service (QoS) to UEs in areas that are seriously impacted by propagation blockage (directly to/from the MBS) such as shadowing and blockage geometry [22], [23], [24]. Within the considered scenario, we suppose that a large antenna array consisting of L-elements is used by the MBS to provide service to K single-antenna users. We also assume that the UEs are grouped into M clusters represented by the set $\mathbf{K_U} = \{\mathcal{K}_1, \ldots, \mathcal{K}_M\}$ with $\mathcal{K}_m = \{1, \ldots, K_m\}, m = 1, \ldots, M$, with cluster having different numbers of users. To support the M clusters of UEs, we use one RIS-equipped UAV working as a small-cell base station where the RIS panel is comprised of N discrete elements to reflect the signal from each group of UEs to the MBS. Hence, in general, we denote with (m, k)-th UE as the k-th UE of the m-th group with $m = 1, \ldots, M$ and $k \in \mathcal{K}_m$. We use $u_{m,k}$ as the user association indicator to denote whether the kth UE of the m-th cluster offloads its computing task to the MEC server as follow:

$$u_{m,k} = \begin{cases} 1 & \text{if computing task offloading is needed,} \\ 0 & \text{otherwise.} \end{cases} \tag{1}$$

We denote $u_m = [u_{m,k}]_{k=1}^{K_m}$ the association vector within the cluster, while $\mathbf{u} = [u_m]_{m=0}^{M}$ the entire user-association matrix. As the RIS-equipped UAV reaches the m-th cluster, users that needs to offload a task to the MBS are served according to time division multiple access (TDMA) technique. In this case, the main functionality of the RIS is to steer the beam from the ground user to the MBS. In this way we guarantee that RIS will only reflect the desired signal towards the MBS and no signal form other users [25], [26].

B. CHANNEL MODEL

By considering a 3D Cartesian coordinate system, we indicate the MBS's position, the UAV-RIS position, and users' positions as, (x_0, y_0, H_0), (x_U, y_U, H_U) and $(x_k, y_k, 0)$, $k = 1, 2, \ldots, K$, respectively. Within this notation, H_0 represents the MBS's antenna height while H_U is the height at which the RIS-equipped UAV is flying. These are supposed to be retrieved by the usage of the Global Positioning System (GPS) and locally stored at the MBS. Without loss of generality, we also assume the existence of a line-of-sight (LoS) communication between the MBS and the UAV-RIS, meaning that the path loss between the MBS and the UAV-RIS can be modelled by using free-space path loss model [27] as follow:

$$\beta_{m,0} = \frac{\beta_0}{d_{m,0}^2 + (H_0 - H_m)^2}, \; m = 1, \ldots, M, \tag{2}$$

where $d_{m,0} = \sqrt{(x_0 - x_m)^2 + (y_0 - y_m)^2}$, d_0 is the reference distance, and β_0 represents the power gain of wireless channel. In this case, H_m represents the height of the UAV when it flies on top of the m-th cluster as explained later in section II-E.

As regards the communication channel between the UAV-RIS and the (m, k)-th UE as the air-to-ground (ATG) channels, they are more complicated because of the propagation blockage effects. To this end, we have the path-loss formulation including the air-to-air (ATA) link and the air-to-ground (ATG) link are denoted as follows [28]:

$$\beta_{m,k} = PL_{m,k} + \eta_{LoS} P_{m,k}^{LoS} + \eta_{NLoS} P_{m,k}^{NLoS}, \tag{3}$$

Let us denote the average additional losses for the LoS and NLoS paths as η_{LoS} and η_{NLoS}, respectively. Since we can derive the distance path loss as

$$PL_{m,k} = 10 \log \left(\frac{4\pi f_c D_{m,k}}{c} \right)^{\alpha}, \tag{4}$$

Here, we have α as the path loss exponent with the value $\alpha \geq 2$, likely, c and f_c are the speed of light in m/s unit and the carrier frequency in Hz unit, respectively. Let us consider the Euclidean distance from the UAV-RIS to the (m, k)-th UE and the Euclidean distance from the MBS to the $(0, k)$th UE as $d_{m,k}$, then, we have $D_{m,k} = \sqrt{d_{m,k}^2 + H_m^2}$. To this end, we have the probability of LoS given as follows [29]

$$P_{m,k}^{LoS} = \frac{1}{1 + a \exp\left[-b\left(\arctan\left(\frac{H_m}{d_{m,k}}\right) - a\right)\right]} \tag{5}$$

where the values of both constants a and b depend on the environment. Then, we can express $P_{m,k}^{NLoS} = 1 - P_{m,k}^{LoS}$.

For the UEs that need the help of the RISs to reach the MBS, the small-scale fading coefficients for the channels from the (m, k)-th UE to the UAV-RIS and the UAV-RIS to the MBS ($m \in \mathcal{M}, k \in \mathcal{K}_m$), denoted by $\mathbf{h}_{m,k} \in \mathbb{C}^{N \times 1}$ and $\mathbf{h}_{m,0}^H \in \mathbb{C}^{N \times L}$, respectively. It worth to be noted that the coefficients are assumed as independent and identically distributed (i.i.d.) random variables with zero mean and unit variance, while the superscript H denotes the conjugate transpose operation. Furthermore, we denote $\mathbf{H}_{m,k} \in \mathbb{C}^{N \times 1}$ and $\mathbf{H}_{m,0}^H \in \mathbb{C}^{L \times N}$ as the channel matrix from the (m, k)-th UE to the UAV-RIS and the UAV-RIS to the MBS, respectively, where $\mathbf{H}_{m,k} = \sqrt{\beta_{m,k}} \mathbf{h}_{m,k}$ and $\mathbf{H}_{m,0}^H = \sqrt{\beta_{m,0}} \mathbf{h}_{m,0}^H$. Hence, the cascaded channel matrix of

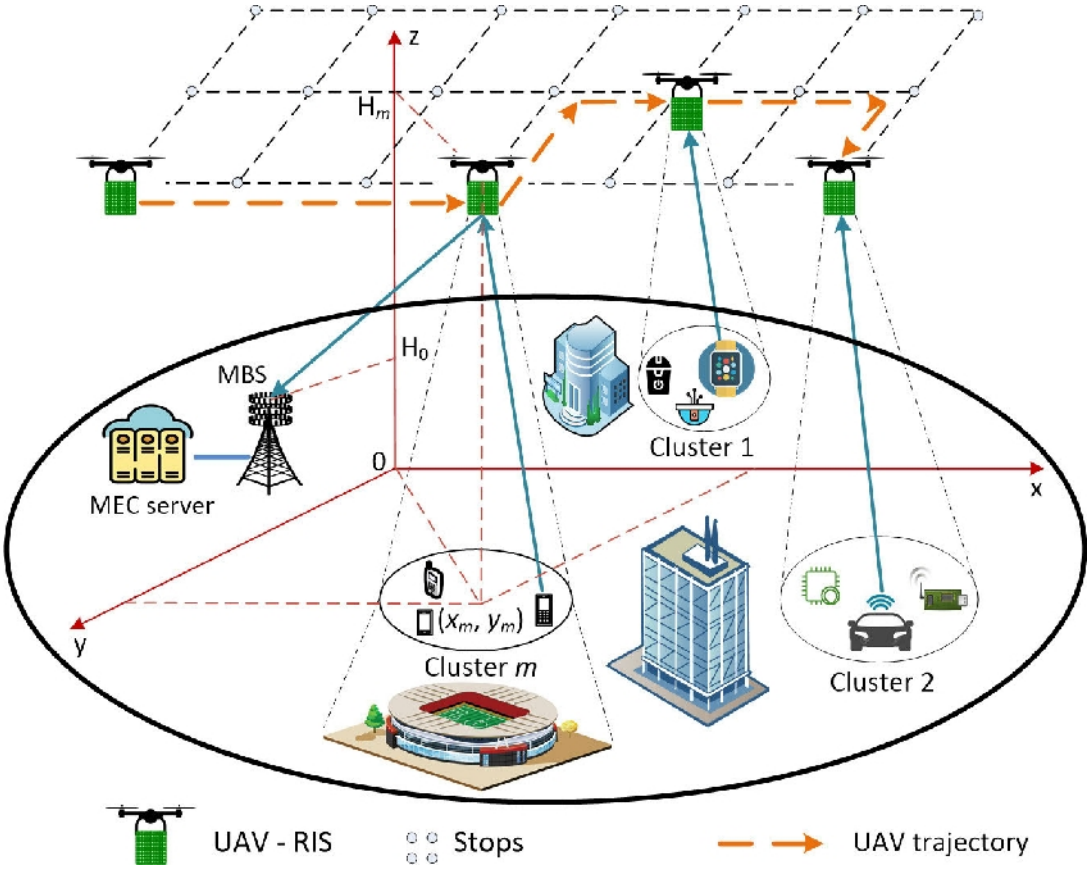

FIGURE 1. Illustration of a MEC system with UAV-RIS.

the link from the (m, k)-th UE to the MBS via the UAV-RIS, $\mathbf{G}_{m,k} \in \mathbb{C}^{L\times 1}$, can be shown as [23]

$$\mathbf{G}_{m,k} = \mathbf{H}_{m,0}^H \Phi_m \mathbf{H}_{m,k}, \ m \in \mathcal{M}, \tag{6}$$

where $\Phi_m = diag[\phi_{1m}, \phi_{2m}, \ldots, \phi_{Nm}]$ is the phase shift matrix at the UAV-RIS; $\phi_{nm} = \alpha_{nm} e^{j\theta_{nm}}$ with $\alpha_{nm} \in [0, 1]$ and $\theta_{nm} \in [0, 2\pi]$ $(\forall n = 1, 2, \ldots, N, \ m \in \mathcal{M})$ denotes the reflection amplitude and phase shift of the n-th reflecting element, respectively. Assuming that only the phase of reflected signals is changed by the RIS reflecting elements, then we can set $\alpha_{nm} = 1$ [30].

C. TRANSMISSION SCHEME

Since the (m, k)-th UE in the m-th group does not have a direct link with the MBS due to propagation blockage such as large buildings, it offloads its computing task to the MBS, it transmits the signal to the MBS via the RIS-equipped UAV. Hence, the signal received at the MBS from the (m, k)-th UE can be expressed as:

$$y_{m,k} = \sqrt{P_{m,k}} \mathbf{G}_{m,k}^H \boldsymbol{f}_{m,k} s_{m,k} + \underbrace{+ \sum_{l=1, l\neq k}^{K_m} \sqrt{P_{l,m}} \mathbf{G}_{l,m}^H \boldsymbol{f}_{l,m} s_{l,m}}_{\text{intra-cell interference}} + n_0, \tag{7}$$

where $P_{m,k}$ is the transmit power of the (m, k)-th UE; $\boldsymbol{f}_{m,k} \in \mathbb{C}^{L\times 1}$ is the beamforming vector of the MBS with respect to the (m, k)-th UE; $s_{m,k}$ is offloading information transmitted by the (m, k)-th UE with $||s_{m,k}||^2 \leq 1$; $n_0 \sim \mathcal{CN}(0, \sigma_0^2)$ is the AWGN at the MBS. The maximum transmit power of the (m, k)-th UE is denoted as $P_{m,k}^{max}$. The first term in (7) denotes the signal transmitted from the (m, k)-th UE via the RIS panel. On the other hand, since the users within the same cluster are supposed to transmit to the MBS at the same time, the second term in (7) represents the intra-cell interference inflicted by the other UEs in the m-th group. To overcome the interference in (7), we apply zero-forcing (ZF) technique [31]. More specifically, we define $\mathbf{G}_m = \left[\mathbf{G}_{m,1}, \ldots, \mathbf{G}_{m,K_m}\right] \in \mathbb{C}^{L\times K_m}$ $(m = 0, 1, \ldots, M)$. As illustrated in [32] and [33], eigenvalue distribution of the square matrix $\mathbf{G}_m^H \mathbf{G}_m \in \mathbb{C}^{K_m \times K_m}$ becomes more deterministic as L increases. Based on this favorable propagation of the mMIMO system, we develop a beamforming vector $\boldsymbol{f}_{m,k}$ by applying ZF as follows. Let

$$\bar{\boldsymbol{f}}_m = \mathbf{G}_m (\mathbf{G}_m^H \mathbf{G}_m)^{-1}, \tag{8}$$

where $\bar{\boldsymbol{f}}_m = \left[\bar{\boldsymbol{f}}_{m,1}, \cdots, \bar{\boldsymbol{f}}_{m,K_m}\right] \in \mathbb{C}^{L\times K_m}$, $\bar{\boldsymbol{f}}_{m,k} \in \mathbb{C}^{L\times 1}$, $m = 0, 1, \ldots, M$, $k \in \mathcal{K}_m$. We then normalize $\tilde{\boldsymbol{f}}_{m,k} = \bar{\boldsymbol{f}}_{m,k} / \|\bar{\boldsymbol{f}}_{m,k}\|$ and calculate $\boldsymbol{f}_{m,k}$ as

$$\boldsymbol{f}_{m,k} = \sqrt{p_{m,k}} \tilde{\boldsymbol{f}}_{m,k}, \ m = 0, 1, \ldots, M, \ k \in \mathcal{K}_m, \tag{9}$$

where $p_{m,k}$ is power control coefficient of the (m, k)-th UE.

Hence, the equation (7) becomes

$$y_{m,k} = \sqrt{P_{m,k}}\sqrt{p_{m,k}}\mathbf{G}_{m,k}^H \tilde{\boldsymbol{f}}_{m,k} s_{m,k} + n_0, \tag{10}$$

where the intra-cell interference in (7) has been cancelled.

Let $p_m = [p_{m,k}]_{k=1}^{K_m}$ and $\boldsymbol{p} = [p_m]_{m=0}^{M}$ denote the power control coefficients, and $\Phi = [\Phi_m]_{m=1}^{M}$ denote the phase shifts of RIS panels, the achievable throughput (in bits per second) at the MBS with respect to the transmission of the (m, k)-th UE can be given by

$$R_{m,k}\left(p_{m,k}, \Phi_m\right) = W \log_2\left(1 + \frac{P_{m,k} p_{m,k} \left|\mathbf{G}_{m,k}^H \tilde{\boldsymbol{f}}_{m,k}\right|^2}{\sigma_0^2}\right), \tag{11}$$

where W is the bandwidth allocated to the (m, k)-th UE.

D. OFFLOADING MODEL

In terms of computation modelling, we suppose that a particular task of size $\mathcal{I}_{m,k}$ can be executed either locally by the (m, k)-th UE or remotely through the assistance of the MEC server located within the MBS. To this end, we define two models of the computation latency as detailed below.

1) LOCAL COMPUTING

Indicating with $\mathcal{F}_{m,k}$ represents the number of CPU cycles required to compute each bit of the task by the (m, k)-th UE, the required time to execute the task locally is obtained as [34]:

$$T_{m,k}^l = \frac{\mathcal{I}_{m,k}\mathcal{F}_{m,k}}{c_{m,k}}, \ m = 0, 1, \ldots, M, \ k \in \mathcal{K}_m, \tag{12}$$

where $c_{m,k}$ denotes the maximum computing resource of the (m, k)-th UE.

2) OFFLOADING TO MBS

On the other hand, if the task is offloaded from the (m, k)-th UE to the MBS, we need first to take into account the offloading transmission time expressed as [34]:

$$T_{m,k}^{tx}(p_{m,k}, \Phi_m) = \frac{\mathcal{I}_{m,k}}{R_{m,k}\left(p_{m,k}, \Phi_m\right)}, \tag{13}$$

where $R_{m,k}\left(p_{m,k}, \Phi_m\right)$ is the communication rate expressed in (11). Once the task reaches the MBS, the computing time for the offloaded task at the MBS can be given as

$$T_{m,k}^{com}(\zeta_{m,k}^{bs}) = \frac{\mathcal{I}_{m,k}\mathcal{F}_{m,k}}{\zeta_{m,k}^{bs}}, \ m = 0, 1, \ldots, M, \ k \in \mathcal{K}_m, \tag{14}$$

where $\zeta_{m,k}^{bs}$ denotes the computing capacity of the MBS allocated to process the task of the (m, k)-th UE. For convenience, let $\zeta_m = [\zeta_{m,k}^{bs}]_{k=1}^{K_m}$ and $\zeta = [\zeta_m]_{m=0}^{M}$ denote the MBS computing capacity allocation. From (12)-(14), hence, the total latency for executing the task of the (m, k)-th UE can be written as

$$T_{m,k}^{tot}(p_{m,k}, u_{m,k}, \Phi_m, \zeta_{m,k}^{bs}) = (1 - u_{m,k})T_{m,k}^l + \\ + u_{m,k}\left(T_{m,k}^{tx}(p_{m,k}, \Phi_m) + T_{m,k}^{com}(\zeta_{m,k}^{bs})\right). \tag{15}$$

Algorithm 1 Shortest Trajectory

Require: $(0, 0, H_m)$, (x_m, y_m, H_m), $d_{\max}$
Ensure: $\mathcal{T}$

1: Generate all the permutations of the original stops in the sequence of $\{1, 2, \ldots, M\}$ to obtain the matrix $\mathcal{M}$ of $M!$ rows and M columns. Each permutation is a row representing a potential solution, i.e., flight sequence or a trajectory.
2: **for** each row $\mathcal{R}$ in $\mathcal{M}$ **do**
3: Compute the distance d from the UAV to the final stop
4: **if** $d < d_{\max}$ **then**
5: $\mathcal{T} \leftarrow \mathcal{R}$
6: $d_{\max} = d$
7: **end if**
8: **end for**

Note that we can ignore the time required for transmitting the computation results from the MBS back to the UEs since such latency is much less than the total latency for executing the task [34], [35].

E. CLUSTERS CREATION AND UAV TRAJECTORY

In terms of cluster creation and relative flying path optimization for the UAV we used an approach similar to the one provided in our previous work presented in [36] . More specifically, the creation of the clusters is based on the UE channel gains. Once the clusters are created, in order to save energy, the UAV will fly from its original position $(0, 0, H_0)$ to the closest cluster center within a straight line. Once it reaches the cluster center, it adjusts its flying height H_m within the range (H^{min}, H^{max}) in order to satisfy the QoS requirements as illustrated in our previous work (see Eq (22) of [36].

III. PROBLEM FORMULATION AND PROPOSED APPROACH

For the UAV-RIS assisted MEC model illustrated in Section II, we formulated an optimisation problem aimed at minimizing the total latency for executing the tasks of all the users in the considered area. This will be achieved through the joint optimisation of all the most relevant system variables, i.e., the power allocated by each user ($\boldsymbol{p}$), user association ($\mathbf{u}$), phase shift matrix of the RIS (Φ), and computing resource allocation at the MBS (ζ) subject to the MBS computing resource constraints and QoS requirements. More in detail, such optimisation problem is formulated as follows:

$$\min_{\boldsymbol{p},\mathbf{u},\Phi,\zeta} \sum_{m=0}^{M}\sum_{k=1}^{K_m} T_{m,k}^{tot}\left(p_{m,k}, u_{m,k}, \Phi_m, \zeta_{m,k}^{bs}\right) \tag{16a}$$

$$\text{s.t.} \quad 0 \le p_{m,k} \le 1, \tag{16b}$$

$$R_{m,k}\left(p_{m,k}, \Phi_m\right) \ge \bar{r}_0, \ m = 0, 1, \ldots, M, \ k \in \mathcal{K}_m, \tag{16c}$$

$$0 \le \theta_{nm} \le 2\pi, \forall n = 1, 2, \ldots, N, \ m \in \mathcal{M}, \tag{16d}$$

$$\sum_{k=1}^{K_m} u_{m,k}\zeta_{m,k}^{bs} \leq \zeta_{max}, \tag{16e}$$

where $u_{m,k}$ represents the user association coefficient as defined in (1). As regards the other constraints, (16b) represents the range of the power that can be used by each user, while (16c) the QoS requirements of each user in terms of minimum achievable uplink rate $\bar{r}_0$. On the other hand, the value range of each RIS phase-shift coefficient is expressed through constraint (16d). Finally, (16e) reflects the limit of computing resources at the MEC server that can be allocated at each UE.

Due to the non-convexity of such sum-latency minimization problem, we proposed a three-step optimisation framework that firstly finds the optimal value of power coefficient for a fixed value for RIS coefficients, ζ and $\mathbf{u}$. Subsequently, we formulate another optimisation problem aimed at finding the optimal value of the phase-shift coefficient at RIS. Finally, the optimal value for ζ is obtained. All the optimisation steps, described within the subsequent subsections, are repeated at each iteration until a stop condition is met (see Algorithm 4).

A. OPTIMAL POWER ALLOCATION

For any given $\mathbf{u}, \Phi, \zeta$, the original problem (16) can be reformulated as follow:

$$\min_{\boldsymbol{p}} \sum_{m=0}^{M}\sum_{k=1}^{K_m} T_{m,k}^{tot}\left(p_{m,k}\right)$$
$$\text{s.t. (16b), (16c).} \tag{17a}$$

To solve this new problem with make use of the following inequality [37], [38]:

$$f(x) = \log_2(1+\frac{1}{x}) \geq \hat{f}(x), \tag{18}$$

where $\hat{f}(x)$ is defined as follow:

$$\begin{aligned}\hat{f}(x) =& \log_2(1+\frac{1}{\bar{x}}) + \left(\frac{\partial f(\bar{x})}{\partial x}\right)(x-\bar{x}) \\ =& \log_2\left(1+\frac{1}{\bar{x}}\right) + \frac{1}{1+\bar{x}} - \frac{x}{(1+\bar{x})\bar{x}}.\end{aligned} \tag{19}$$

To this end, it is worth mentioning that (18) holds $\forall x > 0$ and $\forall \bar{x} > 0$. In our case, at the i-th iteration of Algorithm 2, both x and $\bar{x}$ are represented by the following quantities: WW

$$x = \frac{\sigma_0^2}{P_{m,k}p_{m,k}\left|\mathbf{G}_{m,k}^H \tilde{\boldsymbol{f}}_{m,k}\right|^2},$$
$$\bar{x} = x^{(i)} = \frac{\sigma_0^2}{P_{m,k}p_{m,k}^{(i)}\left|\mathbf{G}_{m,k}^H \tilde{\boldsymbol{f}}_{m,k}\right|^2},$$

These are used for approximating the throughput of each (m,k)-th UE as follows:

$$R_{m,k}\left(p_{m,k}\right) \geq \hat{R}_{m,k}^{(i)}\left(p_{m,k}\right), \ \forall m \in \mathcal{M}, \ \forall k \in \mathcal{K}_m, \tag{20}$$

with

$$\hat{R}_{m,k}^{(i)}\left(p_{m,k}\right) = W\left(\log_2\left(1+\frac{1}{\bar{x}}\right) + \frac{1}{1+\bar{x}} - \frac{x}{(1+\bar{x})\bar{x}}\right). \tag{21}$$

Subsequently, by introducing a new variables $\mathbf{r} \triangleq \{r_{m,k}\}$ $(\forall m \in \mathcal{M}, \forall k \in \mathcal{K})$, that satisfies the condition $\frac{1}{R_{m,k}(p_{m,k})} \leq r_{m,k}$, we can provide the following upper-bound for the objective function $T_{m,k}^{tot}\left(r_{m,k}\right)$:

$$\begin{aligned}T_{m,k}^{tot}\left(r_{m,k}\right) &\leq \hat{T}_{m,k}^{tot}\left(r_{m,k}\right) \\ &= (1-u_{m,k})T_{m,k}^{l} + u_{m,k}\left(r_{m,k}\mathcal{I}_{m,k} + T_{m,k}^{com}\right).\end{aligned} \tag{22}$$

As a result, we can rewrite the problem (17) as

$$\min_{\boldsymbol{p},\mathbf{r}} \sum_{m=0}^{M}\sum_{k=1}^{K_m} \hat{T}_{m,k}^{tot}\left(r_{m,k}\right) \tag{23a}$$
$$\text{s.t.} \quad p_{m,k} \leq 1, \ P_{m,k} \leq P^{\max}, \tag{23b}$$
$$\hat{R}_{m,k}^{(i)}\left(p_{m,k}\right) \geq \bar{r}_0, \tag{23c}$$
$$\frac{1}{\hat{R}_{m,k}^{(i)}} \leq r_{m,k}, \ m = 0, 1, \ldots, M, \ k \in \mathcal{K}_m, \tag{23d}$$

Consequently, problem (23) is now in the form of a standard convex optimisation problem that can be efficiently solved by using convex optimisation solvers like CVX [39]. The proposed power allocation procedure for solving problem (23) is summarised in Algorithm 2.

Algorithm 2 Optimal Power Allocation Procedure for Solving Problem (23)

Input:
Set $\mathbf{u}$, Φ, ζ and initial point $\boldsymbol{p}^{(0)}$;
Set the tolerance $\varepsilon = 10^{-3}$, the maximum iterations $I_{max} = 20$ to stop the algorithm;
for $m = 1$ to M do
Set $i = 0$
repeat
Solve problem (23) for the feasible solution $(\boldsymbol{p}^{(i+1)})$;
Set $i = i + 1$;
until Convergence or $i > I_{max}$;
end for
Output: Optimal power control coefficients $(\boldsymbol{p}^*)$

B. PHASE SHIFT OPTIMISATION

At this stage, we use the values of $\boldsymbol{p}$ obtained through Algorithm 2, while $\mathbf{u}$, and ζ have the same original value set during the power resource optimisation. Then, for these fixed values problem (16) can be rewritten as:

$$\min_{\Phi} \sum_{m=0}^{M}\sum_{k=1}^{K_m} T_{m,k}^{tot}\left(\Phi_m\right) \tag{24a}$$
$$\text{s.t.} \quad \text{(16c), (16d).} \tag{24b}$$

In this case, for a given beamforming vector ($\boldsymbol{f}_{m,k},\ \forall n = 1, 2, \ldots, N,\ m \in \mathcal{M}$) at the MBS, the main objective will be to search the optimal set of phase-shift coefficients for the RIS. Indicating the vector of phase-shift coefficients as $v_m = [v_m^1, \ldots, v_m^N]^H$ with $v_m^n = e^{j\theta_{nm}}$ ($\forall n = 1, 2, \ldots, N$), one can easily notice that the constraint (16d) is equivalent to the unit-modulus constraint i.e., $|v_m^n|^2 = 1$ [40]. At this stage, by defining the new variables $\chi_{m,k} = diag(\mathbf{H}_{m,0}^H)\mathbf{H}_{m,k}\tilde{\boldsymbol{f}}_{m,k}$, that leads to $\mathbf{H}_{m,0}^H \Phi_m \mathbf{H}_{m,k}\tilde{\boldsymbol{f}}_{m,k} = v_m^H \chi_{m,k}$, and by also applying the approximation as in (20)-(21), we can define the following inequality:

$$R_{m,k}\left(\Phi_m\right) \geq \tilde{R}_{m,k}^{(i)}\left(\Phi_m\right),\ \forall m \in \mathcal{M},\ \forall k \in \mathcal{K}_m, \tag{25}$$

where

$$\tilde{R}_{m,k}^{(i)}\left(\Phi_m\right) = W\left(\log_2\left(1+\frac{1}{\bar{y}}\right) + \frac{1}{1+\bar{y}} - \frac{y}{(1+\bar{y})\bar{y}}\right),$$

$$y = \frac{\sigma_0^2}{P_{m,k}p_{m,k}\left|v_m^H \chi_{m,k}\right|^2},$$

$$\bar{y} = y^{(i)} = \frac{\sigma_0^2}{P_{m,k}p_{m,k}\left|v_m^{H(i)} \chi_{m,k}\right|^2}.$$

In addition, by the mean of introducing a new variable $\tilde{\mathbf{r}} \triangleq \{\tilde{r}_{m,k}\}$ ($\forall m \in \mathcal{M}, \forall k \in \mathcal{K}$), that satisfies $\frac{1}{R_{m,k}(\Phi_m)} \leq \tilde{r}_{m,k}$, the objective function $T_{m,k}^{tot}\left(\tilde{r}_{m,k}\right)$ can be upper-bounded as:

$$T_{m,k}^{tot}\left(\tilde{r}_{m,k}\right) \leq \tilde{T}_{m,k}^{tot}\left(\tilde{r}_{m,k}\right) = \\ = (1-u_{m,k})T_{m,k}^{l} + u_{m,k}\left(\tilde{r}_{m,k}\mathcal{I}_{m,k} + T_{m,k}^{com}\right). \tag{26}$$

As result, problem (24) can be reformulated as follow:

$$\min_{v_m,\ \tilde{\mathbf{r}},\ m\in\mathcal{M}} \sum_{m=0}^{M}\sum_{k=1}^{K_m} \tilde{T}_{m,k}^{tot}\left(\tilde{r}_{m,k}\right) \tag{27a}$$

$$\text{s.t.}\quad v_m^H \chi_{m,k}\chi_{m,k}^H v_m \geq \left(2^{\bar{r}_0}-1\right)/a_k,\ m \in \mathcal{M},\ k \in \mathcal{K}_m, \tag{27b}$$

$$|v_m^n|^2 = 1, \forall n = 1, 2, \ldots, N,\ m \in \mathcal{M}, \tag{27c}$$

$$\frac{1}{\tilde{R}_{m,k}^{(i)}} \leq \tilde{r}_{m,k},\ m = 0, 1, \ldots, M,\ k \in \mathcal{K}_m \tag{27d}$$

where the constraint (27b) is equivalent to (16c), and $a_k = P_{m,k}p_{m,k}/\sigma_0^2$. However, the new optimisation problem (27) is still a non-convex quadratically constrained quadratic programming (QCQP) problem. To obtain a more easy formulation, we introduce additional transformations. More specifically, we define $\mathbf{X}_{m,k} = \chi_{m,k}\chi_{m,k}^H$ and $v_m^H \mathbf{X}_{m,k} v_m = tr\left(\mathbf{X}_{m,k} v_m v_m^H\right) = tr\left(\mathbf{X}_{m,k} V_m\right)$ where $V_m = v_m v_m^H$ must satisfy $V_m \succeq 0$ and rank(V_m)=1 [40], [41]. These allow us to obtain the following equivalent transformation for problem (27):

$$\min_{v_m,\ \tilde{\mathbf{r}},\ m\in\mathcal{M}} \sum_{m=0}^{M}\sum_{k=1}^{K_m} \tilde{T}_{m,k}^{tot}\left(\tilde{r}_{m,k}\right) \tag{28a}$$

$$\text{s.t.}\quad tr\left(\mathbf{X}_{m,k} V_m\right) \geq \left(2^{\bar{r}_0}-1\right)/a_k,\ m \in \mathcal{M},\ k \in \mathcal{K}_m, \tag{28b}$$

$$V_{m(n,n)} = 1, \forall n = 1, 2, \ldots, N,\ m \in \mathcal{M}, \tag{28c}$$

$$V_m \succeq 0, \tag{28d}$$

$$\frac{1}{\tilde{R}_{m,k}^{(i)}} \leq \tilde{r}_{m,k},\ m = 0, 1, \ldots, M,\ k \in \mathcal{K}_m, \tag{28e}$$

with $y = \frac{\sigma_0^2}{P_{m,k}p_{m,k}tr\left(\mathbf{X}_{m,k}V_m\right)}$. As one can easily notice, problem (28) is a convex semi-definite program (SDP) [40], [42], and then easy to solve by using CVX. The entire Block Coordinate Descent (BCD)-based procedure for phase shift searching is summarized in Algorithm 3.

Algorithm 3 Phase Shift Searching Procedure for Solving Problem (28)

Input:
Set $\mathbf{u}$, ζ, $\boldsymbol{p}$, and initial $\boldsymbol{f}_{m,k}^{(0)}$.
Set the tolerance $\varepsilon = 10^{-3}$, the maximum iterations $I_{max} = 20$ to stop the algorithm.
for $m = 1$ to M do
  Set $i = 0$
  repeat
    Solve problem (28) for the feasible solution ($\Phi_m^{(i+1)}$).
    Update $\boldsymbol{f}_{m,k}^{(i+1)}$.
    Set $i = i + 1$.
  until Convergence or $i > I_{max}$.
end for
Output: Optimal phase shift (Φ_M^*)

C. COMPUTATION OFFLOADING OPTIMISATION

Finally, using the optimal values of $\boldsymbol{p}$, $\mathbf{u}$, Φ obtained through the optimisation steps described in the previous subsection, we obtain the following optimisation problem with respect to ζ:

$$\min_{\zeta} \sum_{m=0}^{M}\sum_{k=1}^{K_m} T_{m,k}^{tot}\left(\zeta_{m,k}^{bs}\right) \tag{29a}$$

$$\text{s.t. (16e)},$$

which can also be easily through CVX since both the objective function and constraint (16e) are both convex with respect to ζ.

D. ITERATIVE OPTIMISATION ALGORITHM

Finally, we propose an iterative optimisation problem to jointly identify the optimal power allocation, phase shift searching, and computation offloading. The entire optimisation process is summarised in Algorithm 4 showing all the optimisation flow where the solution in each iteration is the initial point in the next iteration.

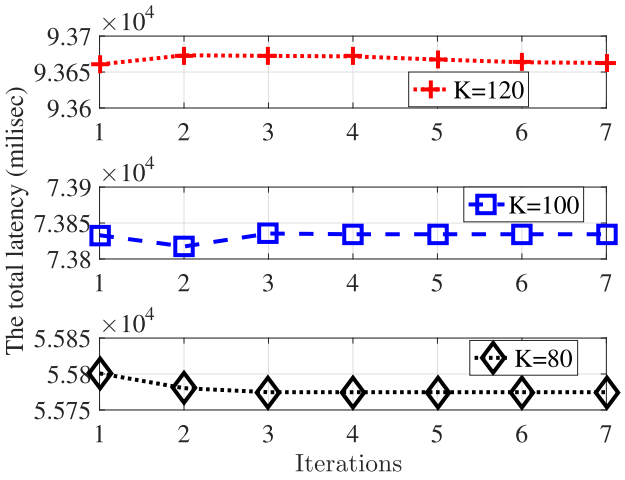

FIGURE 2. Convergence of the proposed optimization framework when changing the number of user K in the communication scenario.

Algorithm 4 Iterative Optimisation Algorithm for Jointly Solving Problem (16)

Input:
Set $\mathbf{u}$, Φ, ζ and initial point $\boldsymbol{p}^{(0)}, \boldsymbol{f}_{m,k}^{(0)}, \zeta^{(0)}$;
Set the tolerance $\varepsilon = 10^{-3}$, the maximum iterations $I_{max} = 20$ to stop the algorithm;
Set $j = 0$
repeat
Solve problem (23) for the feasible solution $(\boldsymbol{p}^{(j+1)})$;
Solve problem (28) for the feasible solution $(\boldsymbol{f}_{m,k}^{(j+1)})$;
Solve problem (29) for the feasible solution $(\zeta^{(j+1)})$;
Set $j = j + 1$;
until Convergence or $j > I_{max}$;
Output: $(\boldsymbol{p}^*, \boldsymbol{f}_{m,k}^*, \zeta^*)$

IV. SIMULATION RESULTS

This section provides the performance evaluations in terms of convergence of the proposed optimisation framework, as well as in term of the latency minimization when compared with other conventional scheme where only optimal resource allocation at the MEC server is performed, i.e., neither optimal power allocation nor phase-shift coefficients optimisation for the RIS is performed. To carry out these performance evaluations we considered the following parameters. The MBS is supposed to be placed at the center of a circular area and provide service to users located within 500 m distance through a direct connection. In addition, it is also assumed that there is a need to serve users distant up to 2000 m from the MBS. Within such a scenario, the 3D Cartesian coordinates of the MBS are (0, 0, 30), while all the UEs are randomly distributed within the whole area. As regards the RIS-equipped UAV, it is supposed to fly within this area and an altitude range (H^{min}, H^{max}) set to (50, 150) m. In terms of physical transmission parameters, in addition to the ones adopted in [37], it is assumed that each UE can use up to $P_{m,k}^{max} = 30$ dBm for the uplink transmissions over a communication channel with central frequency $f_c = 2.4$ GHz, bandwidth $W = 1$ MHz, and subject to white noise spectral density $\sigma_0^2 = -130$ dBm/Hz. In terms of QoS requirements, the minimum achievable rate for each UE in uplink is set to $\bar{r}_0 = 1$ Mbps. In terms of task computing, we assume that each UE needs to perform task computing, either locally or at the MBS, with a size of $D_m = 100$ kB and inner computation complexity of $\mathcal{F}_{m,k} = 600$ cycles/bit. The maximum computing resource (CPU cycle frequency) of the MEC server and the UEs are $\zeta_{max} = 30$ Giga cycles/s and $c_{m,k} = 0.5$ Giga cycles/s, respectively [43].

Under these assumptions, we evaluate the performance of our proposed optimisation framework, when compared with the conventional scheme detailed above, in terms of:

- Capability of reducing the total network latency, which is defined as $\sum_{m=0}^{M} \sum_{k=1}^{K_m} T_{m,k}^{tot}$.
- Ability of reducing the worst-case total latency defined as $\sum_{m=0}^{M} \max_{k \in \mathcal{K}_m} \{T_{m,k}^{tot}\}$.

A. CONVERGENCE ANALYSIS

The convergence characteristics of the proposed optimization framework have been evaluated by changing the number of users considered within the communication scenario. This is because, an increase in the number of users, corresponds to an increase in the variables to optimize, i.e., the number of clusters, power coefficients at the MBS, optimal sets of phase-shift coefficients, and computation optimal computation policy at the MEC server.

As illustrated in Figure 2 the proposed optimization framework requires only a few iterations to solve the optimization problem in line with Algorithm 4. More specifically, when $K = 80$ or $K = 100$ the algorithm converges after 3 iterations, while it requires more iterations when $K = 120$. This is because, as stated before, an increase in users corresponds to an increase in the optimization variables, which in turn requires more time for the algorithm to converge.

On the other hand, one can easily notice how an increase in the number of users also corresponds to an increase in the total latency for the worst-case user. This can be explained by the fact that, for a fixed amount of communication resources at the MBS and computation resources at the MEC, the higher the number of users that offload their tasks to the MEC server, the lower the resources that will be allocated to each user, requiring then more time at the MEC server receive the task, complete it and transmit back to the user. These aspects will be more evident in the next subsections.

B. THE WORST-CASE LATENCY VS COMPUTATION COMPLEXITY $\mathcal{F}_{M,K}$

In Figure 3, we demonstrate the total network latency of all UEs for different values of $\mathcal{F}_{m,k}$, with $K = 80$ and $\zeta_{max} = 30$ Giga cycles/s. The total latency is evaluated with difference values of CPU cycles, $\mathcal{F}_{m,k}$, ranging from 600 to

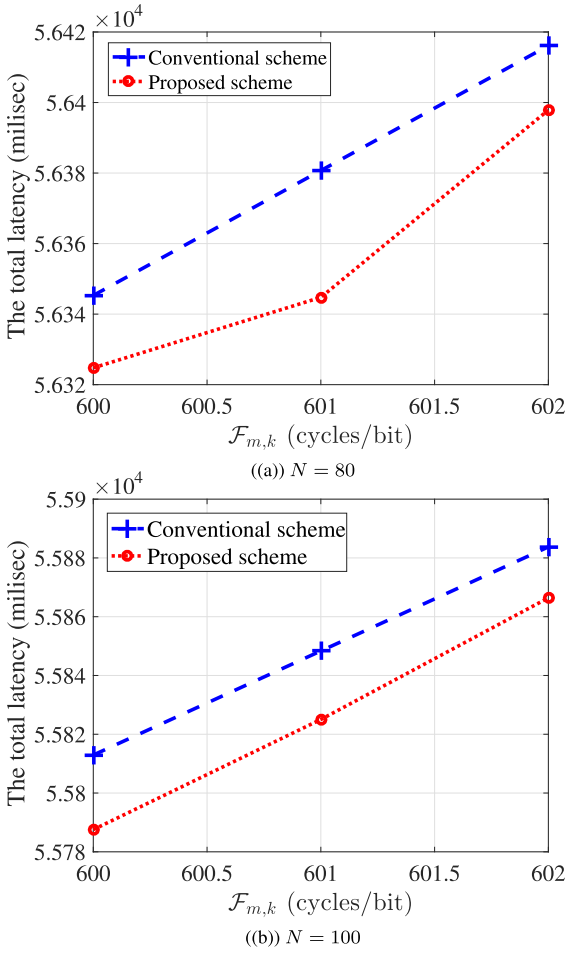

FIGURE 3. The total network latency according to different resource allocation schemes versus a range of $\mathcal{F}_{m,k}$, with $K = 80$ and $\zeta_{max} = 30$ Giga cycles/s.

602 cycles/bit, while the number of reflecting elements of RIS is $N = 80$ and $N = 100$, respectively.

Particularly, Figures 3(a) and 3(b) show the outperformance of the proposed method compared with the conventional scheme in terms of the total network latency. For instance, with $N = 80$ and $\mathcal{F}_{m,k} = 600$, the total latency with the proposed scheme and the conventional scheme is 5.632×10^4 ms and 5.635×10^4 ms, respectively. Moreover, the higher the number of reflecting elements, the lower the total network latency. To this end, it is worth mentioning that these results are valid for the range of considered reflective elements and do not represent a general rule [44] Furthermore, in Figure 4, we evaluate the total worst-case latency with different values of CPU cycles, $\mathcal{F}_{m,k}$. From the figure, we can observe that the total worst-case latency increases with the number of CPU cycles required to compute each bit of the task, i.e., the task complexity. Hence, the UEs should offload their local computing tasks to the MEC server to reduce the latency. By making jointly optimal power allocation, phase shift, and computation offloading, the proposed scheme can provide a better performance than the conventional scheme in terms of the total worst-case latency. On the other hand, when $\mathcal{F}_{m,k}$

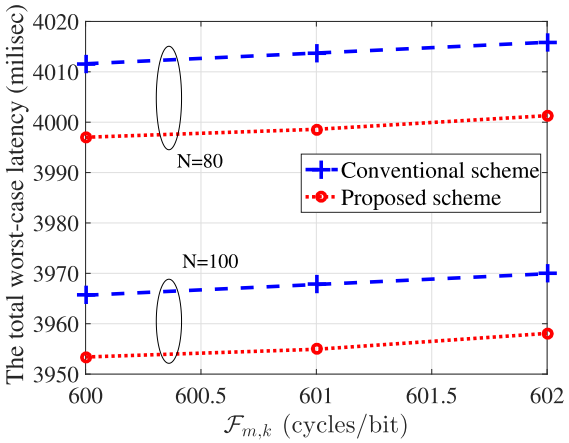

FIGURE 4. The total worst-case latency according to different resource allocation schemes versus a range of $\mathcal{F}_{m,k}$, with $K = 80$ and $\zeta_{max} = 30$ Giga cycles/s.

increases from 600 to 602 Giga cycles/s, with $N = 80$, the total worst-case latency with the proposed scheme goes up from approximately 3997 ms to 4001 ms while with $N = 100$, the total worst-case latency rises from some 3953 ms to 3958 ms, respectively. This again confirms that, increasing the number of RIS elements within the considered range, provides improvements in the system performance in terms of reduced latency.

C. THE WORST-CASE LATENCY VS COMPUTATION CAPABILITIES ζ_{MAX}

In Figure 5, we evaluate the total network latency with the proposed scheme in comparison with the conventional scheme for a range of computing capacity of MBS (Mega cycles/s), ζ_{max}. The number of UEs and CPU cycles is set at $K = 80$ and $\mathcal{F}_{m,k} = 600$ cycles/bit, respectively. Specifically, Figure 5 shows how an increase in the number of RIS elements and the computing capacity of MBS improves the total network latency. As observed from Figure 5, the total latency goes down remarkably with the computing capacity of MBS, ζ_{max}. For example, with $N = 80$, when the computing capacity of MBS increases from 4.5×10^4 to 4.53×10^4, the total latency reduces from 1.826×10^4 to 1.816×10^4. On the other hand, in Figure 6, we prove the benefits of the proposed method for UAV-RIS aided MEC system in terms of the total worst-case latency. It can be seen that, in general, the total worst-case latency declines significantly with the increase of the computing capacity. Most importantly, the proposed scheme always achieves a better latency performance than that of the benchmark. This again proves the efficiency of the proposed optimisation scheme i.e., jointly optimal power allocation, phase shift, and computation offloading for the UAV-RIS aided MEC system.

D. EXPERIMENTAL SUMMARY

In light of illustrations and relative discussions provided in subsections IV-B and IV-C, one can easily notice how the proposed optimization scheme is able to reach higher

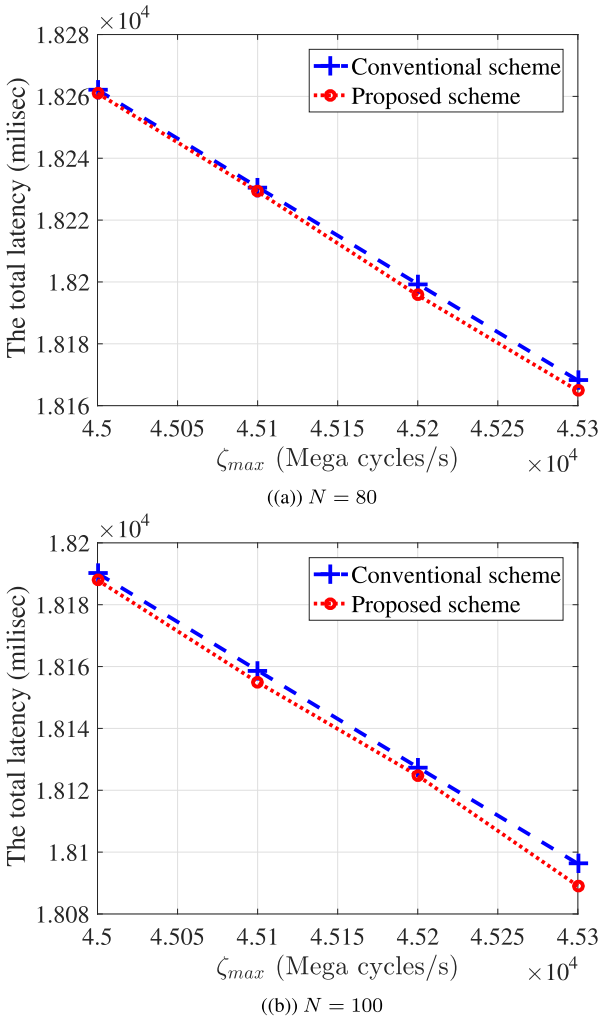

FIGURE 5. The total network latency according to different resource allocation schemes versus various values of ζ_{max}, with $K = 80$ and $\mathcal{F}_{m,k} = 600$ cycles/bit.

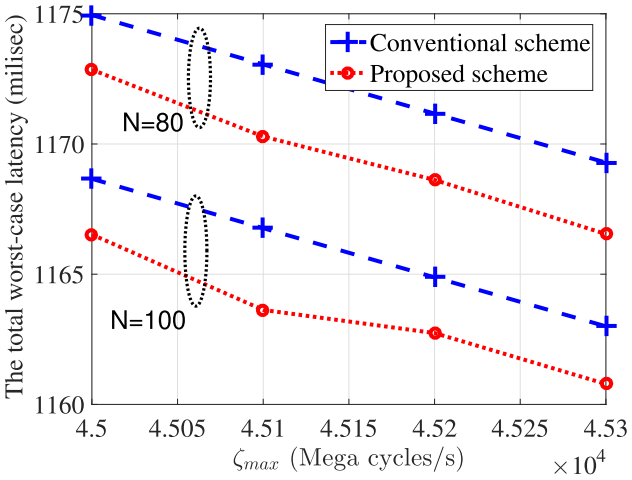

FIGURE 6. The total worst-case latency according to different resource allocation schemes versus various values of ζ_{max}, with $K = 80$ and $\mathcal{F}_{m,k} = 600$ cycles/bit.

performances in terms of reduced network latency when compared with a conventional transmission scheme where neither optimal power allocation at the MBS nor phase-shift coefficients optimisation for the RIS is performed. Indeed, the proposed optimization scheme has been tested within different configurations obtained by varying the main influential parameters of the considered communication scenarios such as the number of reflective elements N at the RIS panel and the computation complexity of the task $\mathcal{F}_{m,k}$ required by each user, and the CPU frequency at the MEC server ζ_{max}. Based on the obtained results we can summarize the main key point of this study as follows:

- In all the considered scenarios, the proposed optimization framework can find the optimal configurations of power allocation at the MBS and phase-shift coefficients for the RIS, as well as optimal path for the UAV, that permits to obtain lower levels of communication latency, while guaranteeing the QoS requirements for each user in the network.
- There is clear evidence that the communication latency increases when the task complexity $\mathcal{F}_{m,k}$ increases, while it decreases with an increase of either the number N of RIS elements or CPU frequency at the MEC server ζ_{max} increases. In any case cases, the proposed framework can provide the optimal resource allocation which minimizes the overall communication latency.
- For the considered scenario, the proposed optimization framework can provide lower levels of communication latency also for the worst-case user. This highlights the importance of how the usage of UAV equipped with RIS panels and joint optimization of UAV path, power allocation at the MBS, and phase-shift coefficients for the reflective elements represents a powerful solution to foster the deployment of 6G-oriented services with low-latency requirements.

The obtained results represent then a clear contribution to the current state of the art of 6G-based communication and services.

V. CONCLUSION

In this paper, we have proposed an MEC system hosted within a massive MIMO base station, serving M groups of users with the assistance of RIS-equipped UAV to enhance the coverage of the whole communication system. For such a communication scenario, we have considered the optimization problem of minimising the total latency for executing tasks of all UEs in the proposed system. More specifically, we have formulated the min-sum latency of all UEs by jointly optimising the user power allocation, user association, phase shift of reflecting elements of RIS, and computing allocation at the MBS subject to the QoS, and the MBS computing capacity. Additionally, we have designed the trajectory for UAV to save total fly time throughout M stops associated with M clusters of UEs for task offloading. The effectiveness of the proposed scheme has been demonstrated through numerical simulations, which highlighted how the

proposed scheme outperforms in terms of reducing the total network latency and the total worst-case latency of all UEs when compared with the conventional scheme. In the future, we plan to investigate the jittering effect of UAVs and extend to multiple UAVs in Internet of Things scenarios. Last but not least, we are also planning to design an optimization algorithm aimed at finding the optimal number of clusters and UAV-related trajectory to minimize the communication latency and save energy on the UAV side.

REFERENCES

[1] *IMT Traffic Estimates for the Years 2020 to 2030*, document ITU-R M.2370-0, Jul. 2015.
[2] W. Jiang, B. Han, M. A. Habibi, and H. D. Schotten, "The road towards 6G: A comprehensive survey," *IEEE Open J. Commun. Soc.*, vol. 2, pp. 334–366, 2021.
[3] H. Viswanathan and P. E. Mogensen, "Communications in the 6G era," *IEEE Access*, vol. 8, pp. 57063–57074, 2020.
[4] W. Saad, M. Bennis, and M. Chen, "A vision of 6G wireless systems: Applications, trends, technologies, and open research problems," *IEEE Netw.*, vol. 34, no. 3, pp. 134–142, May 2020.
[5] F. Guo, F. R. Yu, H. Zhang, X. Li, H. Ji, and V. C. M. Leung, "Enabling massive IoT toward 6G: A comprehensive survey," *IEEE Internet Things J.*, vol. 8, no. 15, pp. 11891–11915, Aug. 2021.
[6] N. Abbas, Y. Zhang, A. Taherkordi, and T. Skeie, "Mobile edge computing: A survey," *IEEE Internet Things J.*, vol. 5, no. 1, pp. 450–465, Feb. 2018.
[7] S. Wang, X. Zhang, Y. Zhang, L. Wang, J. Yang, and W. Wang, "A survey on mobile edge networks: Convergence of computing, caching and communications," *IEEE Access*, vol. 5, pp. 6757–6779, 2017.
[8] D.-B. Ha, V.-T. Truong, and Y. Lee, "Performance analysis for RF energy harvesting mobile edge computing networks with SIMO/MISO-NOMA schemes," *EAI Endorsed Trans. Ind. Netw. Intell. Syst.*, vol. 8, no. 27, Jun. 2021, Art. no. 169425.
[9] L. Lu, G. Y. Li, A. L. Swindlehurst, A. Ashikhmin, and R. Zhang, "An overview of massive MIMO: Benefits and challenges," *IEEE J. Sel. Topics Signal Process.*, vol. 8, no. 5, pp. 742–758, Oct. 2014.
[10] I. Ahmed, H. Khammari, A. Shahid, A. Musa, K. S. Kim, E. De Poorter, and I. Moerman, "A survey on hybrid beamforming techniques in 5G: Architecture and system model perspectives," *IEEE Commun. Surveys Tuts.*, vol. 20, no. 4, pp. 3060–3097, 4th Quart., 2018.
[11] A. Masaracchia, Y. Li, K. K. Nguyen, C. Yin, S. R. Khosravirad, D. B. D. Costa, and T. Q. Duong, "UAV-enabled ultra-reliable low-latency communications for 6G: A comprehensive survey," *IEEE Access*, vol. 9, pp. 137338–137352, 2021.
[12] S. Basharat, S. A. Hassan, H. Pervaiz, A. Mahmood, Z. Ding, and M. Gidlund, "Reconfigurable intelligent surfaces: Potentials, applications, and challenges for 6G wireless networks," *IEEE Wireless Commun.*, vol. 28, no. 6, pp. 184–191, Dec. 2021.
[13] Y. Li, C. Yin, T. Do-Duy, A. Masaracchia, and T. Q. Duong, "Aerial reconfigurable intelligent surface-enabled URLLC UAV systems," *IEEE Access*, vol. 9, pp. 140248–140257, 2021.
[14] K. K. Nguyen, A. Masaracchia, V. Sharma, H. V. Poor, and T. Q. Duong, "RIS-assisted UAV communications for IoT with wireless power transfer using deep reinforcement learning," *IEEE J. Sel. Topics Signal Process.*, vol. 16, no. 5, pp. 1086–1096, Aug. 2022.
[15] K. K. Nguyen, A. Masaracchia, and C. Yin, "Deep reinforcement learning for intelligent reflecting surface-assisted D2D communications," *EAI Endorsed Trans. Ind. Netw. Intell. Syst.*, vol. 10, no. 1, p. e1, Jan. 2023.
[16] M. T. Nguyen, E. Garcia-Palacios, T. Do-Duy, O. A. Dobre, and T. Q. Duong, "UAV-aided aerial reconfigurable intelligent surface communications with massive MIMO system," *IEEE Trans. Cognit. Commun. Netw.*, vol. 8, no. 4, pp. 1828–1838, Dec. 2022.
[17] T. Do-Duy, D. V. Huynh, E. Garcia-Palacios, T.-V. Cao, V. Sharma, and T. Q. Duong, "Joint computation and communication resource allocation for unmanned aerial vehicle NOMA systems," in *Proc. IEEE 28th Int. Workshop Comput. Aided Modeling Design Commun. Links Netw. (CAMAD)*, Edinburgh, U.K., Nov. 2023, pp. 1–6.
[18] Y. Wang, J. Niu, G. Chen, X. Zhou, Y. Li, and S. Liu, "RIS-aided latency-efficient MEC HetNet with wireless backhaul," *IEEE Trans. Veh. Technol.*, vol. 73, no. 6, pp. 8705–8719, Jun. 2024.
[19] Y. Xu, T. Zhang, Y. Zou, and Y. Liu, "Reconfigurable intelligence surface aided UAV-MEC systems with NOMA," *IEEE Commun. Lett.*, vol. 26, no. 9, pp. 2121–2125, Sep. 2022.
[20] H. Hu, Z. Sheng, A. A. Nasir, H. Yu, and Y. Fang, "Computation capacity maximization for UAV and RIS cooperative MEC system with NOMA," *IEEE Commun. Lett.*, vol. 28, no. 3, pp. 592–596, Mar. 2024.
[21] Z. Zhai, X. Dai, B. Duo, X. Wang, and X. Yuan, "Energy-efficient UAV-mounted RIS assisted mobile edge computing," *IEEE Wireless Commun. Lett.*, vol. 11, no. 12, pp. 2507–2511, Dec. 2022.
[22] Z. Chu, P. Xiao, M. Shojafar, D. Mi, J. Mao, and W. Hao, "Intelligent reflecting surface assisted mobile edge computing for Internet of Things," *IEEE Wireless Commun. Lett.*, vol. 10, no. 3, pp. 619–623, Mar. 2021.
[23] Q. Wu and R. Zhang, "Beamforming optimization for wireless network aided by intelligent reflecting surface with discrete phase shifts," *IEEE Trans. Commun.*, vol. 68, no. 3, pp. 1838–1851, Mar. 2020.
[24] P. Wang, J. Fang, X. Yuan, Z. Chen, and H. Li, "Intelligent reflecting surface-assisted millimeter wave communications: Joint active and passive precoding design," *IEEE Trans. Veh. Technol.*, vol. 69, no. 12, pp. 14960–14973, Dec. 2020.
[25] T. J. Cui, M. Q. Qi, X. Wan, J. Zhao, and Q. Cheng, "Coding metamaterials, digital metamaterials and programmable metamaterials," *Light: Sci. Appl.*, vol. 3, no. 10, p. e218, Oct. 2014.
[26] H. Taghvaee, A. Cabellos-Aparicio, J. Georgiou, and S. Abadal, "Error analysis of programmable metasurfaces for beam steering," *IEEE J. Emerg. Sel. Topics Circuits Syst.*, vol. 10, no. 1, pp. 62–74, Mar. 2020.
[27] M.-N. Nguyen, L. D. Nguyen, T. Q. Duong, and H. D. Tuan, "Real-time optimal resource allocation for embedded UAV communication systems," *IEEE Wireless Commun. Lett.*, vol. 8, no. 1, pp. 225–228, Feb. 2019.
[28] M. Mozaffari, W. Saad, M. Bennis, and M. Debbah, "Efficient deployment of multiple unmanned aerial vehicles for optimal wireless coverage," *IEEE Commun. Lett.*, vol. 20, no. 8, pp. 1647–1650, Aug. 2016.
[29] A. Al-Hourani, S. Kandeepan, and S. Lardner, "Optimal LAP altitude for maximum coverage," *IEEE Wireless Commun. Lett.*, vol. 3, no. 6, pp. 569–572, Dec. 2014.
[30] X. Xie, F. Fang, and Z. Ding, "Joint optimization of beamforming, phase-shifting and power allocation in a multi-cluster IRS-NOMA network," *IEEE Trans. Veh. Technol.*, vol. 70, no. 8, pp. 7705–7717, Aug. 2021.
[31] H. Q. Ngo, M. Matthaiou, T. Q. Duong, and E. G. Larsson, "Uplink performance analysis of multicell MU-SIMO systems with ZF receivers," *IEEE Trans. Veh. Technol.*, vol. 62, no. 9, pp. 4471–4483, Nov. 2013.
[32] A. Tulino and S. Verdú, *Random Matrix Theory and Wireless Communications*. Delft, The Netherlands: Now Publishers Inc., 2004.
[33] L. D. Nguyen, H. D. Tuan, T. Q. Duong, and H. V. Poor, "Beamforming and power allocation for energy-efficient massive MIMO," in *Proc. 22nd Int. Conf. Digit. Signal Process. (DSP)*, Aug. 2017, pp. 1–5.
[34] Y. Zhou, P. L. Yeoh, C. Pan, K. Wang, M. Elkashlan, Z. Wang, B. Vucetic, and Y. Li, "Offloading optimization for low-latency secure mobile edge computing systems," *IEEE Wireless Commun. Lett.*, vol. 9, no. 4, pp. 480–484, Apr. 2020.
[35] J. Xu and J. Yao, "Exploiting physical-layer security for multiuser multicarrier computation offloading," *IEEE Wireless Commun. Lett.*, vol. 8, no. 1, pp. 9–12, Feb. 2019.
[36] T. Do-Duy, L. D. Nguyen, T. Q. Duong, S. R. Khosravirad, and H. Claussen, "Joint optimisation of real-time deployment and resource allocation for UAV-aided disaster emergency communications," *IEEE J. Sel. Areas Commun.*, vol. 39, no. 11, pp. 3411–3424, Nov. 2021.
[37] L. D. Nguyen, H. D. Tuan, T. Q. Duong, O. A. Dobre, and H. V. Poor, "Downlink beamforming for energy-efficient heterogeneous networks with massive MIMO and small cells," *IEEE Trans. Wireless Commun.*, vol. 17, no. 5, pp. 3386–3400, May 2018.
[38] L. D. Nguyen, H. D. Tuan, T. Q. Duong, and H. V. Poor, "Multi-user regularized zero-forcing beamforming," *IEEE Trans. Signal Process.*, vol. 67, no. 11, pp. 2839–2853, Jun. 2019.
[39] M. Grant and S. Boyd. (Mar. 2014). *CVX: MATLAB Software for Disciplined Convex Programming, Version 2.1*. [Online]. Available: http://cvxr.com/cvx
[40] Q. Wu and R. Zhang, "Intelligent reflecting surface enhanced wireless network via joint active and passive beamforming," *IEEE Trans. Wireless Commun.*, vol. 18, no. 11, pp. 5394–5409, Nov. 2019.
[41] H. Yu, H. D. Tuan, A. A. Nasir, T. Q. Duong, and H. V. Poor, "Joint design of reconfigurable intelligent surfaces and transmit beamforming under proper and improper Gaussian signaling," *IEEE J. Sel. Areas Commun.*, vol. 38, no. 11, pp. 2589–2603, Nov. 2020.

[42] Q. Wu and R. Zhang, "Intelligent reflecting surface enhanced wireless network: Joint active and passive beamforming design," in *Proc. IEEE Global Commun. Conf. (GLOBECOM)*, Dec. 2018, pp. 1–6.
[43] T. Liu, L. Tang, W. Wang, Q. Chen, and X. Zeng, "Digital-twin-assisted task offloading based on edge collaboration in the digital twin edge network," *IEEE Internet Things J.*, vol. 9, no. 2, pp. 1427–1444, Jan. 2022.
[44] D. Tyrovolas, P.-V. Mekikis, S. A. Tegos, P. D. Diamantoulakis, C. K. Liaskos, and G. K. Karagiannidis, "Energy-aware design of UAV-mounted RIS networks for IoT data collection," *IEEE Trans. Commun.*, vol. 71, no. 2, pp. 1168–1178, Feb. 2023.

PHUC Q. TRUONG was born in Can Tho City, Vietnam. He received the B.Eng. degree in electronics and telecommunication engineering and the M.Eng. degree in electronics engineering from Ho Chi Minh City University of Technology and Education, Vietnam, in 2011 and 2014, respectively, where he is currently pursuing the Ph.D. degree with the Faculty of Electrical and Electronics Engineering. He is also a Senior Lecturer with the Faculty of Electrical and Electronics Engineering, Ho Chi Minh City University of Technology and Education. His research interests include convex optimization techniques, heterogeneous networks, the Internet of Things, and intelligent reflecting surfaces (IRS).

TAN DO-DUY (Member, IEEE) received the B.S. degree from the HCMC University of Technology, Ho Chi Minh City, Vietnam, in 2010, the M.S. degree from the Kumoh National Institute of Technology, Gumi, South Korea, in 2013, and the Ph.D. degree from the Autonomous University of Barcelona, Barcelona, Spain, in 2019. He is currently a Lecturer with the Department of Computer and Communication Engineering, Ho Chi Minh City University of Technology and Education, Vietnam. His main research interests include wireless cooperative communications and network coding applications for wireless networking.

ANTONINO MASARACCHIA (Senior Member, IEEE) was a Research Fellow with Queens University Belfast, U.K. He is currently a Lecturer with the Queen Mary University of London. His research interests include 6G networks, digital twin, generative AI and applied machine learning techniques to wireless communications, reconfigurable intelligent surfaces (RIS), UAV-enabled networks, and ultra-reliable low-latency communications (URLLC).

NGUYEN-SON VO (Senior Member, IEEE) received the Ph.D. degree in communication and information systems from the Huazhong University of Science and Technology, China, in 2012. He is currently with the Institute of Fundamental and Applied Sciences, Duy Tan University, Ho Chi Minh City, Vietnam. His research interests include self-powered multimedia wireless communications, quality of experience provision in wireless networks for smart cities, and the IoT for disaster and environment management. He received the Best Paper Award from the IEEE Global Communications Conference, in 2016; and the Prestigious Newton Prize, in 2017. He has been serving as an Associate Editor for IEEE COMMUNICATIONS LETTERS, since 2019; and a Guest Editor for *Physical Communication* (Elsevier), Special Issue on Mission Critical Communications and Networking for Disaster Management, in 2019; *IET Communications*, Special Issue on Recent Advances on 5G Communications, in 2018; *Mobile Networks and Applications* (Springer), Special Issues on The Key Trends in B5G Technologies, Services and Applications, in 2021; *Wireless Communications and Networks for 5G and Beyond*, in 2018; and *Wireless Communications and Networks for Smart Cities*, in 2017.

VAN-CA PHAN received the Ph.D. degree in electronics and radio engineering from Kyung Hee University, Republic of Korea, in 2010. He is currently an Associate Professor with the Department of Computer and Communications Engineering, Faculty of Electrical and Electronics Engineering, Ho Chi Minh City University of Technology and Education, Vietnam. His diverse research interests include wireless and mobile communication networks, heterogeneous networks, game theory, machine learning, reinforcement learning, dynamic programming techniques, the Internet of Things, cyber-physical systems, and embedded systems design, with a particular focus on optimization techniques for wireless and mobile communications.

DAC-BINH HA received the B.S. degree in radio techniques and the M.S. and Ph.D. degrees in communications and information systems from the Huazhong University of Science and Technology (HUST), China, in 1997, 2006, and 2009, respectively. He is currently an Associate Professor with the School of Engineering and Technology, Duy Tan University, Da Nang, Vietnam. His research interests include secure physical layer communications, cooperative communications, cognitive radio, RF energy harvesting networks, B5G/6G networks, mobile edge computing, and quantum computing and communications.

TRUNG Q. DUONG (Fellow, IEEE) is currently a Canada Excellence Research Chair (CERC) and a Full Professor with the Memorial University of Newfoundland, Canada. He is also an Adjunct Chair Professor in telecommunications with Queen's University Belfast, U.K., and the Research Chair of the Royal Academy of Engineering, U.K. His current research interests include quantum communications, wireless communications, signal processing, machine learning, and real-time optimization.

Dr. Duong received the Best Paper Award at the IEEE VTC-Spring 2013, IEEE ICC 2014, IEEE GLOBECOM 2016, 2019, 2022, IEEE DSP 2017, IWCMC 2019, 2023, 2024, and IEEE CAMAD 2023. He was a recipient of the prestigious Newton Prize 2017. He has also received the two prestigious awards from the Royal Academy of Engineering (RAEng): RAEng Research Chair (2021–2025) and the RAEng Research Fellow (2015–2020). He has served as an Editor/a Guest Editor for IEEE TRANSACTIONS ON WIRELESS COMMUNICATIONS, IEEE TRANSACTIONS ON COMMUNICATIONS, IEEE TRANSACTIONS ON VEHICULAR TECHNOLOGY, IEEE COMMUNICATIONS LETTERS, IEEE WIRELESS COMMUNICATIONS LETTERS, IEEE WIRELESS COMMUNICATIONS, *IEEE Communications Magazines*, and IEEE JOURNAL ON SELECTED AREAS IN COMMUNICATIONS.